Scientia Iranica F (2019) 26(6), 3857–3874

Sharif University of Technology
Scientia Iranica
Transactions F: Nanotechnology
http://scientiairanica.sharif.edu

On the vibration of postbuckled functionally graded-carbon nanotube reinforced composite annular plates

R. Gholami[a,*] and R. Ansari[b]

a. *Department of Mechanical Engineering, Lahijan Branch, Islamic Azad University, Lahijan, P.O. Box 1616, Iran.*
b. *Faculty of Mechanical Engineering, University of Guilan, Rasht, P.O. Box 3756, Iran.*

Received 30 May 2018; received in revised form 4 January 2019; accepted 22 April 2019

KEYWORDS
Free vibration of postbuckled nanocomposite annular plate;
Postbuckling behavior;
Carbon nanotube-reinforced composites;
Numerical approach;
GDQ method.

Abstract. This paper studies the free vibration characteristics of post-buckled Functionally Graded (FG) carbon nanotube (CNT) reinforced annular plates. The analysis was performed by employing a Generalized Differential Quadrature (GDQ)-type numerical technique and pseudo-arc length scheme. The material properties of FG-carbon nanotube reinforced composite (CNTRC) plates were evaluated by an equivalent continuum approach based on the modified rule of mixture. The vibration problem was formulated based on the First-order Shear Deformation Theory (FSDT) for moderately thick laminated plates and von Kármán nonlinearity. By employing Hamilton's principle and a variational approach, the nonlinear equations and associated Boundary Conditions (BCs) were derived, which were then discretized by the GDQ method. The postbuckling behavior was investigated by plotting the secondary equilibrium path as the deflection-load curves. Thereafter, the free vibration behaviors of pre- and post-buckled FG-CNTRC annular plates were examined. Effects of different parameters including types of BCs, CNT volume fraction, an outer radius-to-thickness ratio, and an inner-to-outer radius ratio were investigated in detail.

1. Introduction

Since the discovery of carbon nanotubes (CNTs) by Iijima in 1991 [1], considerable advances have been made in the realm of nanotechnology. CNTs are the most extraordinary materials that have been discovered by mankind over the past thirty years. Characterized by extraordinary properties, they have attracted a great deal of attention from the scientific community and beyond [2-5]. These materials have the potential to revolutionize different fields such as medicine, electronics, material science, energy storage, etc. CNTs are reported to enjoy many desired properties such as high tensile strength and Young's modulus. The high strength of CNTs makes them the stiffest known fiber discovered so far. Further, CNTs enjoy excellent thermal and electrical conducting properties and can either show metallic or semi-conducting behavior based on their size, chirality, and purity. Thus, CNTs can be used as reinforcements to enhance the physical and mechanical properties and electrical conductivity of the polymeric structures. Because of some characteristics such as wear and corrosion resistance, low density, light weight, and low cost, polymer-based composites are extensively utilized in the industrial and

*. *Corresponding author. Tel./Fax: +98 1342222906*
Email address: gholami_r@liau.ac.ir (R. Gholami)

doi: 10.24200/sci.2019.51145.2029

engineering usages including marine and automotive technologies, military, and the agricultural industry [6]. The addition of CNTs to polymers may result in the enhancement of many mechanical, electrical, and optical properties of polymer-based nanocomposites. These superior properties make them the best candidate for use in various usages such as actuators, biomedical devices, chemical sensors, and smart memory devices [7,8]. Ajayan et al. [9] fabricated carbon nanotube reinforced composites (CNTRCs) for the first time in 1994. Since then, a number of studies have been performed to utilize CNTs as reinforcement for various materials such as polymer, ceramic, and metals. For instance, Hassanzadeh-Aghdam and Mahmoodi [10] conducted a comprehensive analysis of the mechanical properties of CNT-reinforced metallic nanocomposites by proposing an analytical approach. The effects of CNT volume fraction, interphase, and geometry on the thermal expansion behavior of CNT-reinforced metallic composites were studied by Hassanzadeh-Aghdam et al. [11,12]. Foroughi et al. [13] experimentally examined the influence of CNTs on the mechanical and bioactive properties of bioglass-ionomer cement. Moreover, AfzaliTabar et al. [14] investigated the CNTs and nano-porous graphene on the silica nanohybrid Pickering emulsion. Recently, Rafiee et al. [15] experimentally studied the vibrational and damping behaviors of functionalized multi-walled CNT-reinforced epoxy nanocomposites as the passive damping components.

Among the published papers on the mechanical characteristics of CNT-reinforced composites, the majority have been devoted to the reinforcement of polymers by CNTs [16-24]. This is because of the relative ease of polymer processing, which demands lower temperatures for consolidation compared to metals and ceramic matrix composites. The fascinating mechanical properties of CNTs over carbon fibers have resulted in increasing use of CNT-reinforced composite structures. The main difference between these two types of composites lies in the low quantity of CNTs used in the CNTRCs [25-27]. Meguid and Sun [28] stated that by increasing the CNT volume fraction beyond a specified limit, the mechanical properties of CNTRCs will deteriorate. As a result, the concept of Functionally Graded (FG) materials has been incorporated in the modeling of CNTRCs in order to use CNTs more efficiently in the reinforced composites. The local buckling of CNTRC beams induced by the bending was studied by Vodenitcharova and Zhang [29]. The imperfection sensitivity of the primary resonances of FG-CNTRC beams under periodic transverse loading was examined by Gholami et al. [30]. A Mori-Tanaka-based equivalent model was utilized by Formica et al. [31] to study the free vibration of CNTRC plates. Their study showed that the maximum enhancement of the properties of fiber composites was obtainable by uniformly aligning CNTs with the loading direction. Ansari et al. [32] examined the nonlinear forced vibration of Timoshenko beams made of FG-CNTRCs. Shen and He [33] studied the nonlinear vibration of embedded FG-CNTRC curved panels under thermal loading. It was found that nonlinear vibration behavior of CNTRC panels was considerably affected by the FG-CNT reinforcements. The nonlinear forced vibration of FG-CNTRC rectangular plates based upon Mindlin and Reddy's plate theories was analyzed by Ansari et al. [34,35]. In addition, Ansari et al. [36] analytically studied the postbuckling of piezoelectric FG-CNTRC shells. Lin and Xiang [37] investigated the free vibrational characteristics of SWCNT-reinforced nanocomposite beams. The variational technique of Hamilton's principle and sense of von Kármán's nonlinearity were used to derive the energies of the CNT-reinforced composite beams. Then, by employing the p-Ritz technique, the free vibration problem of the beam was solved. The free vibration of FG-CNTRC cylindrical shells under the thermal loading was analyzed by Song et al. [38] upon employing the assumed modes approach. Mehrabadi et al. [39] examined linear buckling of FG-CNTRC plates under uniaxial and biaxial compression. In a study conducted by Lie et al. [40], free vibrations of SWCNT-reinforced nanocomposite plates were analyzed by the kp-Ritz method. Shen et al. [41] presented a study on the vibrational response of thermally postbuckled sandwich CNTRC plates resting on the elastic mediums. Ahmadi et al. [42] employed a multi-scale finite element procedure to obtain the mechanical properties of carbon fiber-CNT-polyimide nanocomposites and, then, examine the buckling of rods made of these nanocomposites. Recently, according to a variational approach, Gholami and Ansari [43] provided a weak form of mathematical modeling to study the nonlinear resonant responses of shear deformable FG-CNTRC annular sector plates. In addition, the resonance of multi-scale laminated nanocomposite rectangular plates was examined by Gholami et al. [44]. According to the First-order Shear Deformation Theory (FSDT) and Rayleigh-Ritz scheme, the free vibration of nanocomposite spherical panels and shells of revolution was studied by Wang et al. [45].

In this work, upon employing the Generalized Differential Quadrature (GDQ) approach, the free vibration problem of postbuckled FG-CNTRC annular plates with Uniformly Distributed (UD) and FG reinforcements is numerically formulated. It is assumed that the material properties of FG-CNTRCs are obtained by employing a modified rule of mixture-based equivalent model. The postbuckling problem is formulated on the basis of the FSDT with a von Kármán type of kinematic nonlinearity. By applying Hamilton's principle, the nonlinear equations and corresponding

BCs are derived and, then, discretized by the GDQ method. In addition, pseudo-arc length algorithm is employed to find the secondary equilibrium paths of CNTRCs plates. The free vibration of postbuckled CNTRC annular plates is formulated as a standard linear eigenvalue problem. Impacts of design parameters including type of BCs, CNT volume fraction, inner-to-outer radius ratio, and outer radius-to-thickness ratio on the equilibrium postbuckling path and fundamental frequencies in the pre- and post-buckled configurations are investigated.

2. Mathematical formulation

2.1. CNTRCs and material properties

As illustrated in Figure 1, an SWCNT-reinforced composite annular plate with inner radius, a, outer radius, b, and thickness, h, is assumed. It is considered that the SWCNT reinforcements are UD or FG through the thickness. The structure of the CNT significantly affects the properties of the nanocomposites. Thus far, different micromechanical models such as the Mori-Tanaka [46,47] and Voigt models, as well as the rule of the mixture [26,48], have been proposed to obtain the material properties of CNTRCs. The former is used for micro-particles and the latter extensively for the CNTRCs. On a nanoscale, both of these approaches should be extended to capture the small-scale effect. It has been demonstrated that both of Mori-Tanaka and Voigt techniques have an identical level of accuracy in treating the static and dynamic problems of FG ceramic-metal beams [49], plates [50], and shells [51]. Accordingly, applying the modified version of the rule of mixture, one can express the effective Young's and shear modules of CNTRCs as follows [48]:

$$E_{11} = \eta_1 V_{cnt} E_{11}^{cnt} + V_m E^m, \tag{1a}$$

$$\frac{\eta_2}{E_{22}} = \frac{V_{cnt}}{E_{22}^{cnt}} + \frac{V_m}{E^m}, \tag{1b}$$

$$\frac{\eta_3}{G_{12}} = \frac{V_{cnt}}{G_{12}^{cnt}} + \frac{V_m}{G^m}. \tag{1c}$$

By considering this point that, through theformulations, sub-/super-scripts "m" and "cnt" signify the matrix and CNT, respectively, in Eq. (1), G and E represent shear and Young's modules, and η_j $(j = 1, 2, 3)$ identifies the CNT efficiency parameter, which is attributed to the scale-dependent properties. It is notable that η_j will be later obtained by matching the material properties achieved from the Molecular Dynamics (MD) simulations with those obtained from the rule of mixture. In addition, V_{cnt} and V_m denote the volume fractions of CNT and mixture, respectively, and have the following relationship as follows:

$$V_{cnt} + V_m = 1. \tag{2}$$

The FG-CNTRCs are supposed to be in two different configurations, namely O and X types. For convenience, in the following, the two types of FG-CNTRCs are indicated by FGO and FGX. For the case, the FG-CNTRC is referred to as FGO, and the middle surface of the composite is CNT-rich, while, for the FGX, both outer and inner faces are CNT-rich. In this study, the UD, FGO, and FGX distributions of CNTs are of special concern and are expressed as below [48]:

$$\text{UD}: V_{cnt} = V_{cnt}^*, \tag{3a}$$

$$\text{FGO}: V_{cnt} = 2\left(1 - \frac{2\,|z|}{h}\right) V_{cnt}^*, \tag{3b}$$

$$\text{FGX}: V_{cnt} = \frac{4\,|z|}{h} V_{cnt}^*, \tag{3d}$$

where:

$$V_{cnt}^* = \frac{\Lambda_{cnt}}{\Lambda_{cnt} + \left(\frac{\rho^{cnt}}{\rho^m}\right) - \left(\frac{\rho^{cnt}}{\rho^m}\right)\Lambda_{cnt}}. \tag{4}$$

In the preceding equation, Λ_{cnt} is the mass fraction of CNT, and ρ denotes the mass density. Similar to the previous case, effective Poisson's ratios ν and ρ are obtained by Wang and Shen [52]:

$$\nu_{12} = V_{cnt}\nu_{12}^{cnt} + V_m \nu^m, \nu_{21} = \nu_{12} E_{22}/E_{11}, \tag{5}$$

$$\rho = V_{cnt}\rho^{cnt} + V_m \rho^m. \tag{6}$$

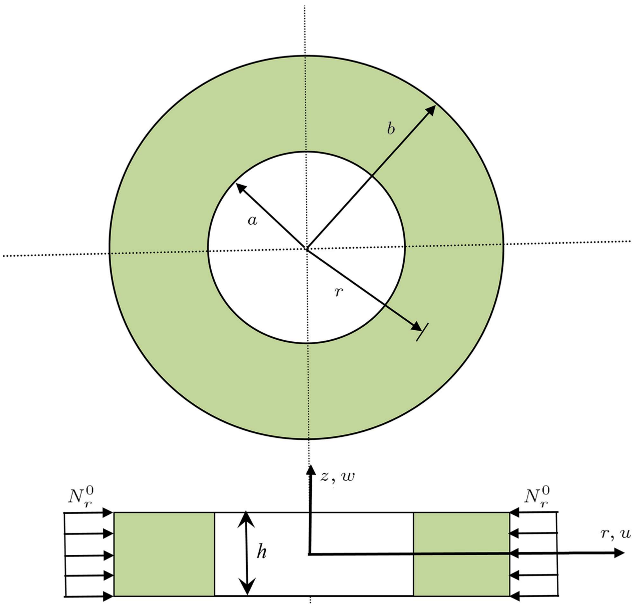

Figure 1. Schematics of an FG-CNTRC annular plate.

2.2. Nonlinear equations of motion and corresponding BCs

Consider a cylindrical coordinate system (r, θ, z) in which its origin is placed at the center of the mid-plane of the FG-CNTRC annular plate, and r, θ, and z-axes denote radial, tangential, and thickness directions, respectively. Considering the axisymmetric deformation, the displacement components, u_r, u_θ and u_z, along r, θ, and z axes, respectively, are obtained by Liew et al. [53]:

$$u_r = u\left(t, r\right) + z\psi_r\left(t, r\right), \quad u_\theta = 0, \; u_z = w\left(t, r\right), \quad (7)$$

where $u(t, r)$ and $w(t, r)$ are the radial and transverse displacement components of middle-plane, respectively, and $\psi_r(t, r)$ is the rotation about θ-axis. In addition, t denotes time. Of note, the displacement field defined in Eq. (7) is based on the FSDT.

By applying Eq. (7), the strain-displacement relations are expressed by:

$$\varepsilon_r = \frac{\partial u}{\partial r} + \frac{1}{2}\left(\frac{\partial w}{\partial r}\right)^2 + z\frac{\partial \psi_r}{\partial r}, \qquad \varepsilon_\theta = \frac{u}{r} + z\frac{\psi_r}{r},$$

$$\varepsilon_{rz} = \varepsilon_{zr} = \frac{1}{2}\left(\psi_r + \frac{\partial w}{\partial r}\right). \quad (8)$$

Additionally, according to the linear elasticity and the von Kármán hypothesis, the nonlinear stress components can be defined by:

$$\begin{Bmatrix} \sigma_r \\ \sigma_\theta \\ \sigma_{rz} \end{Bmatrix} = \begin{bmatrix} Q_{11} & Q_{12} & 0 \\ Q_{12} & Q_{22} & 0 \\ 0 & 0 & Q_{55} \end{bmatrix} \begin{Bmatrix} \varepsilon_r \\ \varepsilon_\theta \\ \varepsilon_{rz} \end{Bmatrix}, \quad (9)$$

where:

$$Q_{11} = \frac{E_{11}}{1 - \nu_{12}\nu_{21}}, \qquad Q_{22} = \frac{E_{22}}{1 - \nu_{12}\nu_{21}},$$

$$Q_{12} = \frac{\nu_{21}E_{11}}{1 - \nu_{12}\nu_{21}}, \qquad Q_{55} = G_{13}. \quad (10)$$

In the previous equation, parameters E_{ij}, G_{ij}, and ν_{ij} are obtained through Eqs. (1) and (5).

Based on the previous discussion, now, the in-plane force resultants (N_r, N_θ), moment resultants (M_r, M_θ), and transverse force resultant (Q_r) are obtainable by:

$$\mathbf{N} = \begin{Bmatrix} N_r \\ N_\theta \end{Bmatrix} = \int_{-h/2}^{h/2} \begin{Bmatrix} \sigma_r \\ \sigma_\theta \end{Bmatrix} dz,$$

$$\mathbf{M} = \begin{Bmatrix} M_r \\ M_\theta \end{Bmatrix} = \int_{-h/2}^{h/2} \begin{Bmatrix} \sigma_r \\ \sigma_\theta \end{Bmatrix} z dz,$$

$$Q_r = \kappa_s \int_{-h/2}^{h/2} \sigma_{rz} dz, \quad (11)$$

where $\kappa_s = \pi^2/12$ denotes the shear correction factor [53]. By inserting Eqs. (9) and (10) into Eq. (11), one obtains:

$$N_r = A_{11}\left[\frac{\partial u}{\partial r} + \frac{1}{2}\left(\frac{\partial w}{\partial r}\right)^2\right] + A_{12}\frac{u}{r} + B_{11}\frac{\partial \psi_r}{\partial r} + B_{12}\frac{\psi_r}{r},$$

$$N_\theta = A_{22}\frac{u}{r} + A_{12}\left[\frac{\partial u}{\partial r} + \frac{1}{2}\left(\frac{\partial w}{\partial r}\right)^2\right] + B_{22}\frac{\psi_r}{r} + B_{12}\frac{\partial \psi_r}{\partial r},$$

$$M_r = B_{11}\left[\frac{\partial u}{\partial r} + \frac{1}{2}\left(\frac{\partial w}{\partial r}\right)^2\right] + B_{12}\frac{u}{r} + D_{11}\frac{\partial \psi_r}{\partial r} + D_{12}\frac{\psi_r}{r},$$

$$M_\theta = B_{22}\frac{u}{r} + B_{12}\left[\frac{\partial u}{\partial r} + \frac{1}{2}\left(\frac{\partial w}{\partial r}\right)^2\right] + D_{22}\frac{\psi_r}{r} + D_{12}\frac{\partial \psi_r}{\partial r},$$

$$Q_r = k_s A_{55}\left(\psi_r + \frac{\partial w}{\partial r}\right), \quad (12)$$

where:

$$\left(A_{ij}, B_{ij}, D_{ij}\right) = \int_{-h/2}^{h/2} Q_{ij}\left(1, z, z^2\right) dz; \quad \left(i, j = 1, 2\right),$$

$$A_{ij} = \int_{-h/2}^{h/2} Q_{ij} dz; \quad \left(i, j = 5\right). \quad (13)$$

The strain energy (Π_s) expression for the FG-CNTRC annular plates takes the following form:

$$\Pi_s = \frac{1}{2}\int_S \int_{-h/2}^{h/2} \sigma_{ij}\varepsilon_{ij} dz dS$$

$$= \frac{1}{2}\int_S \left\{N_r\left[\frac{\partial u}{\partial r} + \frac{1}{2}\left(\frac{\partial w}{\partial r}\right)^2\right] + N_\theta\frac{u}{r} + M_r\frac{\partial \psi_r}{\partial r} + \mathrm{M}_\theta\frac{\psi_r}{r} + Q_r\left(\psi_r + \frac{\partial w}{\partial r}\right)\right\} dS, \quad (14)$$

where S denotes the plate area. The kinetic energy, Π_T, and the potential energy, Π_w, resulting from the applied external radial load, N_r^0, are expressed by:

$$\Pi_T = \frac{1}{2}\int_S \left\{ I_0 \left[\left(\frac{\partial u}{\partial t}\right)^2 + \left(\frac{\partial w}{\partial t}\right)^2 \right] + 2I_1 \frac{\partial \mathrm{u}}{\partial \mathrm{t}}\frac{\partial \mathrm{w}}{\partial \mathrm{t}} + \mathrm{I}_2 \left(\frac{\partial \psi_\mathrm{r}}{\partial \mathrm{t}}\right)^2 \right\} \mathrm{dS}, \tag{15a}$$

$$\Pi_\mathrm{w} = \int_S \left[\frac{1}{2} N_\mathrm{r}^0 \left(\frac{\partial w}{\partial r}\right)^2 \right] dS. \tag{15b}$$

Using Hamilton's principle [54]:

$$\int_{t_1}^{t_2} (\delta \Pi_T - \delta \Pi_s + \delta \Pi_w)\, dt = 0, \tag{16}$$

where δ denotes the variation operator; one can achieve the governing equations and all possible BCs. By inserting Eqs. (14) and (15) into (16), taking the variation of u, w, and ψ_r through the integration by parts, and lastly by equating the coefficients of δu, δw, and $\delta \psi_r$ to zero, the following expressions are obtained for the governing equations of motion (Eqs. (17a)-(17c)) and the BCs (Eqs. (18a)-(18c))

$$\frac{\partial N_r}{\partial r} + \frac{N_r - N_\theta}{r} = I_0 \frac{\partial^2 u}{\partial t^2} + I_1 \frac{\partial \psi_r}{\partial t^2}, \tag{17a}$$

$$\frac{\partial Q_r}{\partial r} + \frac{Q_r}{r} + \frac{1}{r}\frac{\partial}{\partial r}\left(r N_r \frac{\partial w}{\partial r}\right) + N_r^0 \left(\frac{\partial^2 w}{\partial r^2} + \frac{1}{r}\frac{\partial w}{\partial r}\right) = I_0 \frac{\partial^2 w}{\partial t^2}, \tag{17b}$$

$$\frac{\partial M_r}{\partial r} + \frac{M_r - M_\theta}{r} - Q_r = I_2 \frac{\partial \psi_r}{\partial t^2} + I_1 \frac{\partial^2 u}{\partial t^2}, \tag{17c}$$

and:

$$\delta u = 0 \quad \text{or} \quad N_r = 0, \tag{18a}$$

$$\delta w = 0 \quad \text{or} \quad \left(N_r + N_r^0\right) \frac{\partial w}{\partial r} + Q_r = 0, \tag{18b}$$

$$\delta \psi_r = 0 \quad \text{or} \quad M_r = 0. \tag{18c}$$

By inserting Eq. (12) into Eqs. (17), the governing equations are determined in terms of displacement components as follows:

$$A_{11}\left[\frac{\partial^2 u}{\partial r^2} + \frac{1}{r}\frac{\partial u}{\partial r} + \frac{\partial w}{\partial r}\frac{\partial^2 w}{\partial r^2} + \frac{1}{2r}\left(\frac{\partial w}{\partial r}\right)^2 \right] + B_{11}\left(\frac{\partial^2 \psi_r}{\partial r^2} + \frac{1}{r}\frac{\partial \psi_r}{\partial r}\right) - A_{22}\frac{u}{r^2} - B_{22}\frac{\psi_r}{r^2} - \frac{A_{12}}{2r}\left(\frac{\partial w}{\partial r}\right)^2 = I_0 \frac{\partial^2 u}{\partial t^2} + I_1 \frac{\partial \psi_r}{\partial t^2}, \tag{19a}$$

$$k_s A_{55}\left(\frac{\partial^2 w}{\partial r^2} + \frac{1}{r}\frac{\partial w}{\partial r} + \frac{\partial \psi_r}{\partial r} + \frac{\psi_r}{r}\right) + N(w) + N_r^0 \left(\frac{\partial^2 w}{\partial r^2} + \frac{1}{r}\frac{\partial w}{\partial r}\right) = I_0 \frac{\partial^2 w}{\partial t^2}, \tag{19b}$$

$$B_{11}\left[\frac{\partial^2 u}{\partial r^2} + \frac{1}{r}\frac{\partial u}{\partial r} + \frac{\partial w}{\partial r}\frac{\partial^2 w}{\partial r^2} + \frac{B_{11}}{2r}\left(\frac{\partial w}{\partial r}\right)^2 \right] - B_{22}\frac{u}{r^2} - D_{22}\frac{\psi_r}{r^2} + D_{11}\left(\frac{\partial^2 \psi_r}{\partial r^2} + \frac{1}{r}\frac{\partial \psi_r}{\partial r}\right) - \frac{B_{12}}{2r}\left(\frac{\partial w}{\partial r}\right)^2 - k_s A_{55}\left(\psi_r + \frac{\partial w}{\partial r}\right) = I_2 \frac{\partial \psi_r}{\partial t^2} + I_1 \frac{\partial^2 u}{\partial t^2}, \tag{19c}$$

where:

$$N(w) = \left\{ A_{11}\left[\frac{\partial u}{\partial r} + \frac{1}{2}\left(\frac{\partial w}{\partial r}\right)^2 \right] + A_{12}\frac{u}{r} + B_{11}\frac{\partial \psi_r}{\partial r} + B_{12}\frac{\psi_r}{r} \right\} \left(\frac{1}{\mathrm{r}}\frac{\partial w}{\partial r} + \frac{\partial^2 w}{\partial r^2}\right) + \left\{ A_{11}\left(\frac{\partial^2 u}{\partial r^2} + \frac{\partial w}{\partial r}\frac{\partial^2 w}{\partial r^2}\right) + A_{12}\left(\frac{1}{r}\frac{\partial u}{\partial r} - \frac{u}{r^2}\right) + B_{11}\frac{\partial^2 \psi_r}{\partial r^2} + B_{12}\left(\frac{1}{r}\frac{\partial \psi_r}{\partial r} - \frac{1}{r^2}\psi_r\right) \right\} \frac{\partial w}{\partial r}. \tag{20}$$

The BCs provided in Eq. (18) show the possible edge conditions for the FG-CNTRC annular plates. Consequently, the BCs are as follows:

For the simply supported CNTRC annular plates:

$$N_r = w = \mathrm{M}_r = 0. \tag{21a}$$

For clamped CNTRC annular plates:

$$N_r = w = \psi_r = 0. \tag{21b}$$

The following dimensionless quantities are introduced so as to non-dimensionalize the governing equations of motion:

$$\xi = \frac{r}{b}, \quad \eta = \frac{b}{h}, \quad \{u, w\} \to h\{u, w\},$$

$$\psi_r = \psi_r, \quad \bar{N}_r^0 = \frac{N_r^0}{A_{110}}, \quad \tau = \frac{t}{b}\sqrt{\frac{A_{110}}{I_{10}}},$$

$$\{a_{11}, a_{22}, a_{12}, a_{55}\} = \frac{\{A_{11}, A_{22}, A_{12}, A_{55}\}}{A_{110}},$$

$$\{d_{11}, d_{22}, d_{12}, d_{55}\} = \frac{\{D_{11}, D_{22}, D_{12}\}}{A_{110} h^2},$$

$$\{\bar{I}_0, \bar{I}_1, \bar{I}_2\} = \left\{ \frac{I_0}{I_{00}}, \frac{I_1}{I_{00}\mathrm{h}}, \frac{I_2}{I_{00}\mathrm{h}^2} \right\}, \tag{22}$$

where A_{110} and I_{00} show the values of A_{11} and I_0 for a homogeneous matrix plate. Thus, one obtains:

$$a_{11}\left[\frac{\partial^2 u}{\partial\xi^2} + \frac{1}{\xi}\frac{\partial u}{\partial\xi} + \frac{1}{\eta}\frac{\partial w}{\partial\xi}\frac{\partial^2 w}{\partial\xi^2} + \frac{1}{2\eta\xi}\left(\frac{\partial w}{\partial\xi}\right)^2\right]$$
$$+ b_{11}\left(\frac{\partial^2\psi_r}{\partial r^2} + \frac{1}{\xi}\frac{\partial\psi_r}{\partial\xi}\right) - a_{22}\frac{u}{\xi^2} - b_{22}\frac{\psi_r}{\xi^2}$$
$$- \frac{A_{12}}{2\eta\xi}\left(\frac{\partial w}{\partial\xi}\right)^2 = \bar{I}_0\frac{\partial^2 u}{\partial\tau^2} + \bar{\mathrm{I}}_1\frac{\partial\psi_r}{\partial\tau^2}, \tag{23a}$$

$$k_s a_{55}\left(\frac{\partial^2 w}{\partial\xi^2} + \frac{1}{\xi}\frac{\partial w}{\partial\xi} + \eta\frac{\partial\psi_r}{\partial\xi} + \eta\frac{\psi_r}{\xi}\right)$$
$$+ \bar{N}_r^0\left(\frac{\partial^2 w}{\partial\xi^2} + \frac{1}{\xi}\frac{\partial w}{\partial\xi}\right)$$
$$+ \frac{1}{\eta}\left\{a_{11}\left[\frac{\partial u}{\partial\xi} + \frac{1}{2\eta}\left(\frac{\partial w}{\partial\xi}\right)^2\right] + a_{12}\frac{u}{\xi}\right.$$
$$\left. + b_{11}\frac{\partial\psi_r}{\partial\xi} + b_{12}\frac{\psi_r}{\xi}\right\}\left(\frac{1}{\xi}\frac{\partial w}{\partial\xi} + \frac{\partial^2 w}{\partial\xi^2}\right)$$
$$+ \frac{1}{\eta}\left\{a_{11}\left(\frac{\partial^2 u}{\partial\xi^2} + \frac{1}{\eta}\frac{\partial w}{\partial\xi}\frac{\partial^2 w}{\partial\xi^2}\right)\right.$$
$$+ a_{12}\left(\frac{1}{\xi}\frac{\partial u}{\partial\xi} - \frac{u}{\xi^2}\right) + b_{11}\frac{\partial^2\psi_r}{\partial\xi^2}$$
$$\left. + b_{12}\left(\frac{1}{\xi}\frac{\partial\psi_r}{\partial\xi} - \frac{\psi_r}{\xi^2}\right)\right\}\frac{\partial w}{\partial\xi} = \bar{I}_0\frac{\partial^2 w}{\partial\tau^2}, \tag{23b}$$

$$b_{11}\left[\frac{\partial^2 u}{\partial\xi^2} + \frac{1}{\xi}\frac{\partial u}{\partial\xi} + \frac{1}{\eta}\frac{\partial w}{\partial\xi}\frac{\partial^2 w}{\partial\xi^2} + \frac{1}{2\eta\xi}\left(\frac{\partial w}{\partial\xi}\right)^2\right]$$
$$- b_{22}\frac{u}{\xi^2} - d_{22}\frac{\psi_r}{\xi^2} + d_{11}\left(\frac{\partial^2\psi_r}{\partial\xi^2} + \frac{1}{\xi}\frac{\partial\psi_r}{\partial\xi}\right)$$
$$- \frac{d_{12}}{2\eta\xi}\left(\frac{\partial w}{\partial\xi}\right)^2 - k_s a_{55}\eta\left(\eta\psi_r + \frac{\partial w}{\partial r}\right)$$
$$= \bar{I}_2\frac{\partial\psi_r}{\partial\tau^2} + \bar{I}_1\frac{\partial^2 u}{\partial\tau^2}. \tag{23c}$$

Further, by non-dimensionalizing the BCs, the following expressions are obtained for the simply supported (Eq. (24a)) and clamped (Eq. (24b)) BCs:

$$a_{11}\left[\frac{\partial u}{\partial\xi} + \frac{1}{2\eta}\left(\frac{\partial w}{\partial\xi}\right)^2\right] + a_{12}\frac{u}{\xi} + b_{11}\frac{\partial\psi_r}{\partial\xi}$$
$$+ b_{12}\frac{\psi_r}{\xi} = w = 0,$$
$$b_{11}\left[\frac{\partial u}{\partial\xi} + \frac{1}{2\eta}\left(\frac{\partial w}{\partial\xi}\right)^2\right] + b_{12}\frac{u}{\xi} + d_{11}\frac{\partial\psi_r}{\partial\xi}$$
$$+ d_{12}\frac{\psi_r}{\xi} = 0, \tag{24a}$$

$$a_{11}\left[\frac{\partial u}{\partial\xi} + \frac{1}{2\eta}\left(\frac{\partial w}{\partial\xi}\right)^2\right] + a_{12}\frac{u}{\xi} + b_{11}\frac{\partial\psi_r}{\partial\xi} + b_{12}\frac{\psi_r}{\xi}$$
$$= w = \psi_r = 0. \tag{24b}$$

3. GDQ method

The GDQ method as an efficient numerical approach can be utilized for solving the boundary value problems including the ordinary and partial differential equations. Unlike the finite element method that is usually employed for solving the weak form of equations, the GDQ technique represents a powerful tool for solving the equations in the strong form with great efficiency and accuracy using a small number of discrete mesh points [55].

3.1. Introduction

With the aid of the GDQ technique [56-58], the pth order derivative of $g(r)$ is attained in the following form:

$$\left.\frac{\partial^p g(p)}{\partial p^p}\right|_{r=r_i} = \sum_{j=1}^{N} \mathcal{A}_{ij}^r g(r_j), \tag{25}$$

where N is the number of total discrete points. By considering a column vector $\mathbf{F}$:

$$\mathbf{F} = [g_j] = [g(r_j)] = [g(r_1), g(r_2), \ldots, g(r_N)]^T, \tag{26}$$

where $g_j = g(r_j)$ indicates the amount of $g(r)$ at r_j, and an operational matrix of differentiation on the basis of Eq. (25) is achieved as in the following form:

$$\frac{\partial^p}{\partial r^p}(\mathbf{F}) = \mathbf{D}_r^p\mathbf{F} = [D_r^p]_{i,j}\{F_j\}, \tag{27}$$

where:

$$\mathbf{D}_r^p = [D_r^p]_{i,j} = \mathcal{A}_{ij}^p, \quad i, j = 1:N, \tag{28}$$

where $\mathcal{A}_{ij}$ gives the weighting coefficients obtained as by Eq. (29) as shown in Box I, in which $\mathcal{P}(r_i) = \Pi_{j=1;j\neq i}^{N}(r_i - r_j)$, and $\mathbf{I}_r$ denotes an $N \times N$ identity matrix.

$$\mathcal{A}_{ij}^{p}=\begin{cases}\mathbf{I}_r, & r=0\\ \frac{\mathcal{P}(r_i)}{(r_i-r_j)\mathcal{P}(r_j)}, & i\neq j \text{ and } i,j=1,\ldots, N \text{ and } p=1\\ p\left(\mathcal{A}_{ij}^{1}\mathcal{A}_{ii}^{p-1}-\frac{\mathcal{A}_{ij}^{p-1}}{r_i-r_j}\right), & i\neq j \text{ and } i,j=1,\ldots, N \text{ and } p=2,3,\ldots N-1\\ -\sum\limits_{j=1;j\neq i}^{N}\mathcal{A}_{ij}^{p}, & i=j \text{ and } i,j=1,\ldots, N \text{ and } p=1,2,3,\ldots N-1\end{cases} \tag{29}$$

Box I

3.2. Postbuckling analysis

With the aid of Chebyshev-Gauss-Lobatto points as the grid points, the mesh generation can be obtained by:

$$\xi_i=\alpha+\frac{1-\alpha}{2}\left(1-\cos\frac{i-1}{N-1}\pi\right), i=1:N, \tag{30}$$

where $\alpha=a/b$. The discretized form of displacement components is defined as the following vectors:

$$\mathbf{U}^{\mathbf{T}}=[U_1,\ldots,U_N],$$
$$\mathbf{W}^{\mathbf{T}}=[W_1,\ldots,W_N],$$
$$\mathbf{\Psi}^{\mathbf{T}}=[\Psi_1,\ldots,\Psi_{\mathrm{N}},], \tag{31}$$

where $U_i=u(\xi_i), W_i=w(\xi_i), \Psi_i=\psi(\xi_i)$. By assuming $\bar{N}_r^0=-P$, utilizing the GDQ scheme, and discarding the inertia terms, the equilibrium equations are discretized by:

$$a_{11}\Big[\mathbf{D}_\xi^2\mathbf{U}+\mathbf{D}_\xi^1\mathbf{U}\circ\mathbf{A}_1+\frac{1}{\eta}\left(\mathbf{D}_\xi^2\mathbf{W}\right)\circ\left(\mathbf{D}_\xi^1\mathbf{W}\right)$$
$$+\frac{1}{2\eta}\left(\mathbf{D}_\xi^1\mathbf{W}\right)\circ\left(\mathbf{D}_\xi^1\mathbf{W}\right)\circ\mathbf{A}_1\Big]$$
$$+b_{11}\left(\mathbf{D}_\xi^2\mathbf{\Psi}+\mathbf{D}_\xi^1\mathbf{\Psi}\circ\mathbf{A}_1\right)-a_{22}\mathbf{U}\circ\mathbf{A}_2$$
$$-b_{22}\mathbf{\Psi}\circ\mathbf{A}_2-\frac{a_{12}}{2\eta}\left(\mathbf{D}_\xi^1\mathbf{W}\right)\circ\left(\mathbf{D}_\xi^1\mathbf{W}\right)\circ\mathbf{A}_1=\mathbf{0}, \tag{32a}$$

$$\kappa_s a_{55}\left(\mathbf{D}_\xi^2\mathbf{W}+\mathbf{D}_\xi^1\mathbf{W}\circ\mathbf{A}_1\right)$$
$$+\kappa_s a_{55}\eta\left(\mathbf{D}_\xi^1\mathbf{\Psi}+\mathbf{\Psi}\circ\mathbf{A}_1\right)$$
$$-P\left[\mathbf{D}_\xi^2\mathbf{W}+\left(\mathbf{D}_\xi^1\mathbf{W}\right)\circ\mathbf{A}_1\right]$$
$$+\frac{1}{\eta}\Big\{a_{11}\left[\mathbf{D}_\xi^1\mathbf{U}+\frac{1}{2\eta}\left(\mathbf{D}_\xi^1\mathbf{W}\right)\circ\left(\mathbf{D}_\xi^1\mathbf{W}\right)\right]$$
$$+b_{11}\mathbf{D}_\xi^1\mathbf{\Psi}+a_{12}\mathbf{U}\circ\mathbf{A}_1+b_{12}\mathbf{\Psi}\circ\mathbf{A}_1\Big\}$$
$$\circ\left[\mathbf{D}_\xi^2\mathbf{W}+\left(\mathbf{D}_\xi^1\mathbf{W}\right)\circ\mathbf{A}_1\right]$$
$$+\frac{1}{\eta}\Big\{a_{11}\left[\mathbf{D}_\xi^2\mathbf{U}+\frac{1}{\eta}\left(\mathbf{D}_\xi^2\mathbf{W}\right)\circ\left(\mathbf{D}_\xi^1\mathbf{W}\right)\right]$$
$$+a_{12}\left[\mathbf{D}_\xi^1\mathbf{U}\circ\mathbf{A}_1-\mathbf{U}\circ\mathbf{A}_2\right]+b_{11}\mathbf{D}_\xi^2\mathbf{\Psi}$$
$$+a_{12}\left[\mathbf{D}_\xi^1\mathbf{U}\circ\mathbf{A}_1-\mathbf{U}\circ\mathbf{A}_2\right]$$
$$+b_{12}\left[\mathbf{D}_\xi^1\mathbf{\Psi}\circ\mathbf{A}_1-\mathbf{\Psi}\circ\mathbf{A}_2\right]\Big\}\circ\left(\mathbf{D}_\xi^1\mathbf{W}\right)=\mathbf{0}, \tag{32b}$$

$$b_{11}\Big[\mathbf{D}_\xi^2\mathbf{U}+\mathbf{D}_\xi^1\mathbf{U}\circ\mathbf{A}_1+\frac{1}{\eta}\left(\mathbf{D}_\xi^2\mathbf{W}\right)\circ\left(\mathbf{D}_\xi^1\mathbf{W}\right)$$
$$+\frac{1}{2\eta}\left(\mathbf{D}_\xi^1\mathbf{W}\right)\circ\left(\mathbf{D}_\xi^1\mathbf{W}\right)\circ\mathbf{A}_1\Big]$$
$$+d_{11}\left(\mathbf{D}_\xi^2\mathbf{\Psi}+\mathbf{D}_\xi^1\mathbf{\Psi}\circ\mathbf{A}_1\right)-b_{22}\mathbf{U}\circ\mathbf{A}_2$$
$$-d_{22}\mathbf{\Psi}\circ\mathbf{A}_2-\frac{b_{12}}{2\eta}\left(\mathbf{D}_\xi^1\mathbf{W}\right)\circ\left(\mathbf{D}_\xi^1\mathbf{W}\right)\circ\mathbf{A}_1$$
$$-\kappa_s a_{55}\eta\left(\eta\mathbf{\Psi}+\mathbf{D}_\xi^1\mathbf{W}\right)=\mathbf{0}, \tag{32c}$$

where $\circ$ shows the Hadamard product [59] and $\mathbf{A}_i^{\mathbf{T}}=\left[1/\xi_1^i,1/\xi_2^i,\ldots,1/\xi_N^i\right]$. Following the same procedure used for the discretization of the equilibrium equation, one can discretize the BCs (Eqs. (18)) similarly. The set of nonlinear equations of the domain can be defined by:

$$\mathbf{G}:\mathbb{R}^{3N+1}\rightarrow\mathbb{R}^{3N},$$
$$\mathbf{G}\left(P,\mathbf{X}\right)=0,$$
$$\mathbf{X}^{\mathbf{T}}=\left[\mathbf{U}^{\mathrm{T}},\mathbf{W}^{\mathrm{T}},\mathbf{\Psi}^{\mathrm{T}}\right], \tag{33}$$

where parameter P is the axial load.

The previous equation due to the presence of P is a parameterized equation. Here, by employing the pseudo-arc length continuation technique, this equation will be solved. To this end, by substituting the residual of equations relevant to boundaries into the residual of the domain $\mathbf{G}(P,\mathbf{X})$, the edge conditions are satisfied. This assumption implies that the elements of

G related to the grid points must be substituted with those of discretized BCs.

3.3. Vibration study in the postbuckled region

Herein, the aim is to examine the linear free vibration of a buckled CNTRC plate. To accomplish this goal, by introducing small disturbances u_d, w_d, and ψ_d, respectively, around the buckled configurations u_s, w_s, and ψ_s, the time evolution of that disturbance will be obtained as follows:

$$\begin{aligned} u(\xi,\tau) &= u_s(\xi) + u_d(\xi,\tau), w(\xi,\tau) \\ &= w_s(\xi) + w_d(\xi,\tau), \psi_r(\xi,\tau) \\ &= \psi_s(\xi) + \psi_d(\xi,\tau). \end{aligned} \tag{34}$$

Thereafter, by inserting the previous equation into the governing equation and ignoring the nonlinear time-dependent terms, the linear free vibration problem is obtained by:

$$\mathbf{m}\ddot{\mathbf{x}} + \mathbf{k}\mathbf{x} = \mathbf{0}, \tag{35}$$

where dot indicates the derivative with respect to τ, $\mathbf{x}$ denotes the generalized coordinate, and $\mathbf{m}$ and $\mathbf{k}$ are the inertia and stiffness matrices, respectively, which can be determined by:

$$\begin{aligned} &\mathbf{x}^{\mathrm{T}} = [u_d, w_d, \psi_d], \\ &\mathbf{m} = \begin{bmatrix} \bar{I}_0 & 0 & \bar{I}_1 \\ 0 & \bar{I}_0 & 0 \\ \bar{I}_1 & 0 & \bar{I}_2 \end{bmatrix}, \\ &\mathbf{k} = \begin{bmatrix} k_{uu} & k_{uw} & k_{u\psi} \\ k_{wu} & k_{ww} & k_{w\psi} \\ k_{\psi u} & k_{\psi w} & k_{\psi\psi} \end{bmatrix}. \end{aligned} \tag{36}$$

The elements of $\mathbf{k}$ are introduced as follows:

$$\begin{aligned} k_{uu} &= a_{11}\left(\frac{\partial^2}{\partial\xi^2} + \frac{1}{\xi}\frac{\partial}{\partial\xi}\right) - a_{22}\frac{1}{\xi^2}, \\ k_{uw} &= \frac{a_{11}}{\eta}\left[\frac{\partial^2 w_s}{\partial\xi^2}\frac{\partial}{\partial\xi} + \frac{\partial w_s}{\partial\xi}\frac{\partial^2}{\partial\xi^2} + \frac{1}{\xi}\frac{\partial w_s}{\partial\xi}\frac{\partial}{\partial\xi}\right] \\ &\quad - \frac{a_{12}}{\eta\xi}\frac{\partial w_s}{\partial\xi}\frac{\partial}{\partial\xi}, \\ k_{u\psi} &= b_{11}\left(\frac{\partial^2}{\partial\xi^2} + \frac{1}{\xi}\frac{\partial}{\partial\xi}\right) - b_{22}\frac{1}{\xi^2}. \end{aligned} \tag{37a}$$

$$\begin{aligned} k_{wu} &= \frac{1}{\eta}\left(a_{11}\frac{\partial}{\partial\xi} + \frac{a_{12}}{\xi}\right)\left(\frac{1}{\xi}\frac{\partial w_s}{\partial\xi} + \frac{\partial^2 w_s}{\partial\xi^2}\right) \\ &\quad + \frac{1}{\eta}\left\{a_{11}\frac{\partial^2}{\partial\xi^2} + a_{12}\left(\frac{1}{\xi}\frac{\partial}{\partial\xi} - \frac{1}{\xi^2}\right)\right\}\frac{\partial w_s}{\partial\xi}, \\ k_{ww} &= k_s a_{55}\left(\frac{\partial^2}{\partial\xi^2} + \frac{1}{\xi}\frac{\partial}{\partial\xi}\right) \\ &\quad + \frac{a_{11}}{\eta^2}\left(\frac{1}{\xi}\frac{\partial w_s}{\partial\xi} + \frac{\partial^2 w_s}{\partial\xi^2}\right)\frac{\partial w_s}{\partial\xi}\frac{\partial}{\partial\xi} \\ &\quad + \frac{a_{11}}{\eta^2}\left(\frac{\partial w_s}{\partial\xi}\frac{\partial^2}{\partial\xi^2} + \frac{\partial^2 w_s}{\partial\xi^2}\frac{\partial}{\partial\xi}\right)\frac{\partial w_s}{\partial\xi} \\ &\quad + \frac{1}{\eta}\left\{a_{11}\left[\frac{\partial u_s}{\partial\xi} + \frac{1}{2\eta}\left(\frac{\partial w_s}{\partial\xi}\right)^2\right] + a_{12}\frac{u_s}{\xi}\right. \\ &\quad \left. + b_{11}\frac{\partial\psi_s}{\partial\xi} + b_{12}\frac{\psi_s}{\xi}\right\}\left(\frac{1}{\xi}\frac{\partial}{\partial\xi} + \frac{\partial^2}{\partial\xi^2}\right) \\ &\quad - P\left(\frac{\partial^2}{\partial r^2} + \frac{1}{r}\frac{\partial}{\partial r}\right) \\ &\quad + \frac{1}{\eta}\left\{a_{11}\left(\frac{\partial^2 u_s}{\partial\xi^2} + \frac{1}{\eta}\frac{\partial w_s}{\partial\xi}\frac{\partial^2 w_s}{\partial\xi^2}\right)\right. \\ &\quad + a_{12}\left(\frac{1}{\xi}\frac{\partial u_s}{\partial\xi} - \frac{u_s}{\xi^2}\right) + b_{11}\frac{\partial^2\psi_s}{\partial\xi^2} \\ &\quad \left. + b_{12}\left(\frac{1}{\xi}\frac{\partial\psi_s}{\partial\xi} - \frac{\psi_s}{\xi^2}\right)\right\}\frac{\partial}{\partial\xi}, \\ k_{w\psi} &= \frac{1}{\eta}\left(b_{11}\frac{\partial}{\partial\xi} + b_{12}\frac{1}{\xi}\right)\left(\frac{1}{\xi}\frac{\partial w_s}{\partial\xi} + \frac{\partial^2 w_s}{\partial\xi^2}\right) \\ &\quad + \frac{1}{\eta}\left\{b_{11}\frac{\partial^2}{\partial\xi^2} + b_{12}\left(\frac{1}{\xi}\frac{\partial}{\partial\xi} - \frac{1}{\xi^2}\right)\right\}\frac{\partial w_s}{\partial\xi} \\ &\quad + k_s a_{55}\eta\left(\frac{\partial}{\partial\xi} + \frac{1}{\xi}\right), \end{aligned} \tag{37b}$$

$$\begin{aligned} k_{\psi u} &= b_{11}\left(\frac{\partial^2}{\partial\xi^2} + \frac{1}{\xi}\frac{\partial}{\partial\xi}\right) - \frac{b_{22}}{\xi^2}, \\ k_{\psi w} &= \frac{b_{11}}{\eta}\left(\frac{\partial w_s}{\partial\xi}\frac{\partial^2}{\partial\xi^2} + \frac{\partial^2 w_s}{\partial\xi^2}\frac{\partial}{\partial\xi} + \frac{1}{\xi}\frac{\partial w_s}{\partial\xi}\frac{\partial}{\partial\xi}\right) \\ &\quad - \frac{d_{12}}{\eta\xi}\frac{\partial w_s}{\partial\xi}\frac{\partial}{\partial\xi} - k_s a_{55}\eta\frac{\partial}{\partial\xi}, \\ k_{\psi\psi} &= -\frac{d_{22}}{\xi^2} + d_{11}\left(\frac{\partial^2}{\partial\xi^2} + \frac{1}{\xi}\frac{\partial}{\partial\xi}\right) - k_s a_{55}\eta^2. \end{aligned} \tag{37c}$$

Now, by employing the GDQ technique, one can discretize Eq. (35) as follows:

$$\mathbf{M}\ddot{\mathbf{X}} + \mathbf{K}\mathbf{X} = \mathbf{0}, \tag{38}$$

in which:

$$\mathbf{X}^{\mathrm{T}} = \left[\mathbf{U}_d^{\mathrm{T}}, \mathbf{w}_d^{\mathrm{T}}, \mathbf{\Psi}_d^{\mathrm{T}}\right],$$

$$\mathbf{M} = \begin{bmatrix} \bar{I}_0\mathbf{D}_\xi^0 & 0 & \bar{I}_1\mathbf{D}_\xi^0 \\ 0 & \bar{I}_0\mathbf{D}_\xi^0 & 0 \\ \bar{I}_1\mathbf{D}_\xi^0 & 0 & \bar{I}_1\mathbf{D}_\xi^0 \end{bmatrix},$$

$$\mathbf{K} = \begin{bmatrix} \mathbf{K}_{uu} & \mathbf{K}_{uw} & \mathbf{K}_{u\psi} \\ \mathbf{K}_{\mathbf{wu}} & \mathbf{K}_{\mathbf{ww}} & \mathbf{K}_{w\psi} \\ \mathbf{K}_{\psi u} & \mathbf{K}_{\psi w} & \mathbf{K}_{\psi\psi} \end{bmatrix}. \tag{39}$$

The components of $\mathbf{K}$ are determined by:

$$k_{uu} = a_{11}\left(\mathbf{D}_\xi^2 + \mathbf{A}_1\diamondsuit\mathbf{D}_\xi^1\right) - a_{22}\mathbf{A}_2\diamondsuit\mathbf{D}_\xi^0,$$

$$k_{uw} = \frac{a_{11}}{\eta}\left[\left(\mathbf{D}_\xi^2\mathbf{W}_\mathrm{s}\right)\diamondsuit\mathbf{D}_\xi^1 + \left(\mathbf{D}_\xi^1\mathbf{W}_\mathrm{s}\right)\diamondsuit\mathbf{D}_\xi^2 + \mathbf{A}_1\circ\left(\mathbf{D}_\xi^1\mathbf{W}_\mathrm{s}\right)\diamondsuit\mathbf{D}_\xi^1\right] - \frac{a_{12}}{\eta}\left[\mathbf{A}_1\circ\left(\mathbf{D}_\xi^1\mathbf{W}_\mathrm{s}\right)\diamondsuit\mathbf{D}_\xi^1\right],$$

$$k_{u\psi} = b_{11}\left(\mathbf{D}_\xi^2 + \mathbf{A}_1\diamondsuit\mathbf{D}_\xi^1\right) - b_{22}\mathbf{A}_2\diamondsuit\mathbf{D}_\xi^0, \tag{40a}$$

$$k_{wu} = \frac{1}{\eta}\left(a_{11}\mathbf{D}_\xi^1 + a_{12}\mathbf{A}_1\right)\diamondsuit\left(\mathbf{A}_1\circ\left(\mathbf{D}_\xi^1\mathbf{W}_\mathrm{s}\right) + \mathbf{D}_\xi^2\mathbf{W}_\mathrm{s}\right) + \frac{1}{\eta}\left\{a_{11}\mathbf{D}_\xi^2 + a_{12}\left(\mathbf{A}_1\diamondsuit\mathbf{D}_\xi^1 - \mathbf{A}_2\diamondsuit\mathbf{D}_\xi^0\right)\right\}\diamondsuit\left(\mathbf{D}_\xi^1\mathbf{W}_\mathrm{s}\right),$$

$$\begin{aligned} k_{ww} =& k_s a_{55}\left(\mathbf{D}_\xi^2 + \mathbf{A}_1\diamondsuit\mathbf{D}_\xi^1\right) + \frac{a_{11}}{\eta^2}\left(\mathbf{D}_\xi^2\mathbf{W}_s + \mathbf{A}_1\circ\left(\mathbf{D}_\xi^1\mathbf{W}_\mathrm{s}\right)\right)\circ\left(\mathbf{D}_\xi^1\mathbf{W}_\mathrm{s}\right) \\ & \diamondsuit\mathbf{D}_\xi^1 + \frac{a_{11}}{\eta^2}\left(\left(\mathbf{D}_\xi^1\mathbf{W}_\mathrm{s}\right)\diamondsuit\mathbf{D}_\xi^2 + \left(\mathbf{D}_\xi^2\mathbf{W}_\mathrm{s}\right)\diamondsuit\mathbf{D}_\xi^1\right) \\ & \circ\left(\mathbf{D}_\xi^1\mathbf{W}_\mathrm{s}\right) + \frac{1}{\eta}\left\{a_{11}\left[\left(\mathbf{D}_\xi^1\mathbf{U}_\mathrm{s}\right) + \frac{1}{2\eta}\left(\mathbf{D}_\xi^1\mathbf{W}_\mathrm{s}\right)\circ\left(\mathbf{D}_\xi^1\mathbf{W}_\mathrm{s}\right)\right] + a_{12}\mathbf{A}_1 \right. \\ & \left. \circ\left(\mathbf{D}_\xi^0\mathbf{U}_\mathrm{s}\right) + b_{11}\mathbf{D}_\xi^1\mathbf{\Psi}_\mathrm{s} + b_{12}\mathbf{A}_1\circ\left(\mathbf{D}_\xi^0\mathbf{\Psi}_\mathrm{s}\right)\right\} \diamondsuit\left(\mathbf{D}_\xi^2 + \mathbf{A}_1\diamondsuit\mathbf{D}_\xi^1\right) \\ & + \frac{1}{\eta}\left\{a_{11}\left(\mathbf{D}_\xi^2\mathbf{U}_\mathrm{s} + \frac{1}{\eta}\left(\mathbf{D}_\xi^1\mathbf{W}_\mathrm{s}\right)\circ\left(\mathbf{D}_\xi^2\mathbf{W}_\mathrm{s}\right)\right) + a_{12}\left(\mathbf{A}_1\circ\left(\mathbf{D}_\xi^1\mathbf{U}_\mathrm{s}\right) - \mathbf{A}_2\circ\left(\mathbf{D}_\xi^0\mathbf{U}_\mathrm{s}\right)\right) \right. \\ & \left. + b_{11}\mathbf{D}_\xi^2\mathbf{\Psi}_\mathrm{s} + b_{12}\left(\mathbf{A}_1\circ\left(\mathbf{D}_\xi^1\mathbf{\Psi}_\mathrm{s}\right) - \mathbf{A}_2\circ\left(\mathbf{D}_\xi^0\mathbf{\Psi}_\mathrm{s}\right)\right)\right\}\diamondsuit\mathbf{D}_\xi^1 - P\left(\mathbf{D}_\xi^2 + \mathbf{A}_1\diamondsuit\mathbf{D}_\xi^1\right), \end{aligned} \tag{40b}$$

$$\begin{aligned} k_{w\psi} =& k_s a_{55}\eta\left(\mathbf{D}_\xi^1 + \mathbf{A}_1\right) + \frac{1}{\eta}\left\{b_{11}\mathbf{D}_\xi^1 + b_{12}\mathbf{A}_1\right\}\diamondsuit\left(\mathbf{D}_\xi^2\mathbf{W}_s + \mathbf{A}_1\circ\mathbf{D}_\xi^1\mathbf{W}_s\right) \\ & + \frac{1}{\eta}\left\{b_{11}\mathbf{D}_\xi^2 + b_{12}\left(\mathbf{A}_1\diamondsuit\mathbf{D}_\xi^1 - \mathbf{A}_2\diamondsuit\mathbf{D}_\xi^0\right)\right\}\diamondsuit\left(\mathbf{D}_\xi^1\mathbf{W}_\mathrm{s}\right), \end{aligned}$$

$$k_{\psi u} = b_{11}\left(\mathbf{D}_\xi^2 + \mathbf{A}_1\diamondsuit\mathbf{D}_\xi^1\right) - b_{22}\mathbf{A}_2\diamondsuit\mathbf{D}_\xi^0,$$

$$k_{\psi w} = \frac{b_{11}}{\eta}\left(\mathbf{D}_\xi^1\mathbf{W}_s\diamondsuit\mathbf{D}_\xi^2 + \mathbf{D}_\xi^2\mathbf{W}_s\diamondsuit\mathbf{D}_\xi^1 + \mathbf{A}_1\circ\left(\mathbf{D}_\xi^1\mathbf{W}_\mathrm{s}\right)\diamondsuit\mathbf{D}_\xi^1\right) - \frac{d_{12}}{\eta}\mathbf{A}_1\circ\left(\mathbf{D}_\xi^1\mathbf{W}_\mathrm{s}\right)\diamondsuit\mathbf{D}_\xi^1 - k_s a_{55}\eta\mathbf{D}_\xi^1,$$

$$k_{\psi\psi} = -d_{22}\mathbf{A}_2 + d_{11}\left(\mathbf{D}_\xi^2 + \mathbf{A}_1\diamondsuit\mathbf{D}_\xi^1\right) - k_s a_{55}\eta^2\mathbf{D}_\xi^0, \tag{40c}$$

where $\diamondsuit$ represents the SJT product (SJT is the abbreviation of Shanghai Jiao Tong Univ.) [59,60]. By considering the harmonic solution of the form $\mathbf{X} = \tilde{\mathbf{X}}e^{i\omega\tau}$, Eq. (39) turns into:

$$-\omega^2\mathbf{M}\tilde{\mathbf{X}} + \mathbf{K}\tilde{\mathbf{X}} = \left(\mathbf{K} - \omega^2\mathbf{M}\right)\tilde{\mathbf{X}} = \mathbf{0}, \tag{41}$$

where ω denotes the non-dimensional frequency.

Substitution of the BCs into $\mathbf{K}$ and $\mathbf{M}$ and the rearrangement of the discretized equations and the associated BCs yield the following eigenvalue problem:

$$\begin{bmatrix} \mathbf{K}_{dd} & \mathbf{K}_{db} \\ \mathbf{K}_{bd} & \mathbf{K}_{bb} \end{bmatrix}\begin{bmatrix} \tilde{\mathbf{X}}_d \\ \tilde{\mathbf{X}}_b \end{bmatrix} = \begin{bmatrix} \omega^2\mathbf{M}_{dd}\tilde{\mathbf{X}}_d \\ \{\mathbf{0}\} \end{bmatrix}, \tag{42}$$

where subscripts d and b are the domain and boundary mesh grid points, respectively.

Eq. (42) can be uncoupled through the following expressions:

$$\begin{cases} \left(\mathbf{K}_{dd} - \mathbf{K}_{db}(\mathbf{K}_{bb})^{-1}\mathbf{K}_{bd}\right)\tilde{\mathbf{X}}_d = \omega^2\mathbf{M}_{dd}\tilde{\mathbf{X}}_d \\ \tilde{\mathbf{X}}_b = (\mathbf{K}_{bb})^{-1}\mathbf{K}_{bd}\tilde{\mathbf{X}}_d. \end{cases} \tag{43}$$

Now, $\omega_i\ (i = 1, 2, 3, \ldots)$ and their corresponding mode shapes $\tilde{\mathbf{X}}^T = \left[\tilde{\mathbf{X}}_d^T, \tilde{\mathbf{X}}_b^T\right]$ can be achieved by finding a solution to Eq. (43).

4. Numerical results and discussion

The formulation and solution procedure developed in the previous sections are utilized to present the numerical results for the postbuckling behavior and the free vibration of the FG-CNTRC annular plates. Effects of various factors on the static equilibrium postbuckling path and frequencies are shown by conducting a non-dimensional study. Poly methyl methacrylate (PMMA) with $\nu^m = 0.34, \rho^m = 1150$ kg/m^3, $E^m =$ 2.5 GPa [26] and armchair (10,10) SWCNTs with $\nu^{cnt} = 0.175, \mathrm{G}_{12}^{cnt} = 1.9445$ TPa, $\mathrm{E}_{11}^{cnt} =$ 5.6466 TPa, $\mathrm{E}_{22}^{cnt} = 7.08$ TPa, $\rho^{cnt} = 1400$ kg/m^3 at room temperature (300 K) [61] are selected as matrix and reinforcements, respectively.

Furthermore, the values of CNT efficiency parameters η_1, η_2, and η_3 for three different CNT volume fractions are considered as follows [26]:

$$V_{cnt}^* = 0.12: \quad \eta_1 = 0.137, \quad \eta_2 = 1.022\ , \eta_3 = 0.715,$$

$$V_{cnt}^* = 0.17: \quad \eta_1 = 0.142, \quad \eta_2 = 1.626\ , \eta_3 = 1.138,$$

$$V_{cnt}^* = 0.28: \quad \eta_1 = 0.141, \quad \eta_2 = 1.585\ , \eta_3 = 1.109.$$

In what follows, a sequence of letters including "SS" and "C" is used to represent the simply supported and clamped BCs, respectively.

To provide a convergence study and illustrate the accuracy of mathematical modeling, solution procedure, and numerical results, the natural frequency parameters of isotropic annular plates are provided in Table 1. It can be seen that the results are converged by increasing N and are in excellent agreement with those of Liew et al. [53]. In this study, $N = 21$ is used in all computational efforts. In addition, in Table 2, the critical buckling load parameters associated with various inner-to-outer radius ratios are compared with those given in [62], illustrating very well agreement.

Depicted in Figure 2 are the static equilibrium postbuckling paths as the maximum non-dimensional deflection, $w_{\max}$, versus the non-dimensional compressive radial load (Non. dim. radial load; $P = \bar{P}/A_{110}$ where $\bar{P}$ is the dimensional compressive radial load) for the three different prescribed distributions of CNTs in the CNTRC annular plates corresponding to four various combinations of simply supported and clamped edge supports. According to this figure, it is revealed that for a fixed value of the radial load, the maximum deflection, $w_{\max}$, corresponding to an FGO-CNTRC annular plate is larger than those of the other two types of CNTRC plates; the FGO-CNTRC annular has the lowest critical buckling load and the highest critical buckling load, and the maximum load-carrying capacity belongs to the FGX distribution pattern. It can be concluded from this figure that the addition of more CNTs to the upper and lower surfaces of FG-CNTRC annular plates results in a considerable increase in the total stiffness of system and induces more resistance against bending. In addition, it is observed that the FG-CNTRC plates with C-C edge conditions have minimum values of maximum deflection and, subsequently, maximum values of critical buckling load, whereas, for the case of the FG-CNTRC annular plates with fully simply supported edges, an opposite trend is seen. The dependence of the non-dimensional frequency (Non. dim. frequency: $\omega = \bar{\omega} b\sqrt{I_{00}/A_{110}}$ where $\bar{\omega}$ denotes the natural frequency) upon the non-dimensional compressive radial load in the pre- and post-buckled states is exhibited in Figure 3. Based on the results exhibited in Figure 3, it can be concluded that the fundamental frequencies of FG-CNTRC annular plates in the pre-

Table 2. Comparison of critical buckling load parameter ($\tilde{P}_{cr} = \bar{P}_{cr} b^2/D_{110}$) of C-C isotropic annular plates ($\nu = 0.3, b/h = 20$).

a/b	Present	Ref. [62]
0.2	59.922	60.01
0.3	76.633	76.77
0.4	101.812	102.05

Table 1. Convergence of the frequency parameters $\left(\tilde{\omega} = \bar{\omega} b^2\sqrt{I_{00}/D_{110}}\right)$ of isotropic annular plates with different BCs ($\nu = 0.3, b/h = 5, a/b = 0.5$).

BCs	Mode	N						Ref. [53]
		5	7	9	11	13	21	
SS-SS	1	31.3583	31.7365	31.7292	31.7292	31.7292	31.7292	31.87
	2	104.3532	89.9127	89.8677	89.8647	89.8647	89.8647	90.64
SS-C	1	41.2354	41.2906	41.2883	41.2883	41.2883	41.2883	41.62
	2	109.4586	94.3543	94.2975	94.2913	94.2914	94.2914	95.27
C-SS	1	37.5501	38.0643	38.0538	38.0538	38.0538	38.0538	38.36
	2	107.2712	92.9592	92.8525	92.8512	92.8512	92.8512	93.78
C-C	1	47.7424	47.8078	47.8099	47.8099	47.8099	47.8099	48.31
	2	110.4921	96.4347	96.2918	96.2885	96.2886	96.2886	97.39

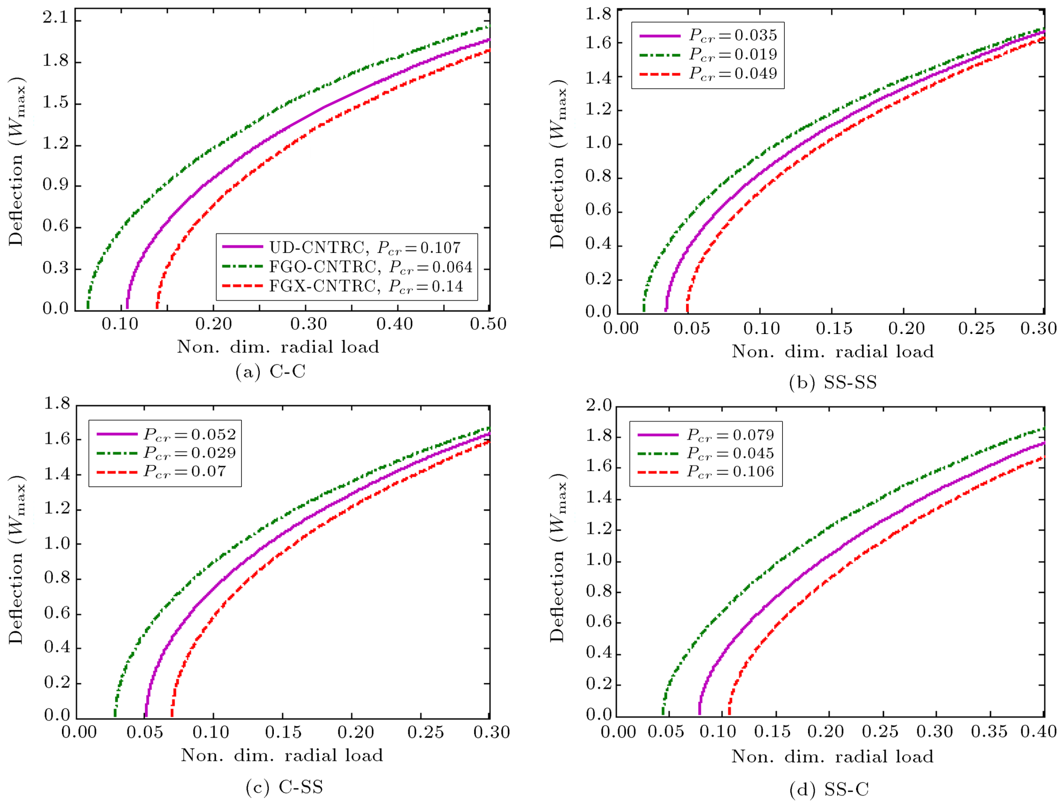

Figure 2. Equilibrium postbuckling path of FG-CNTRC annular plates for three different distributions of the CNTs ($b/h = 40, V_{cnt}^* = 0.17, a/b = 0.2$).

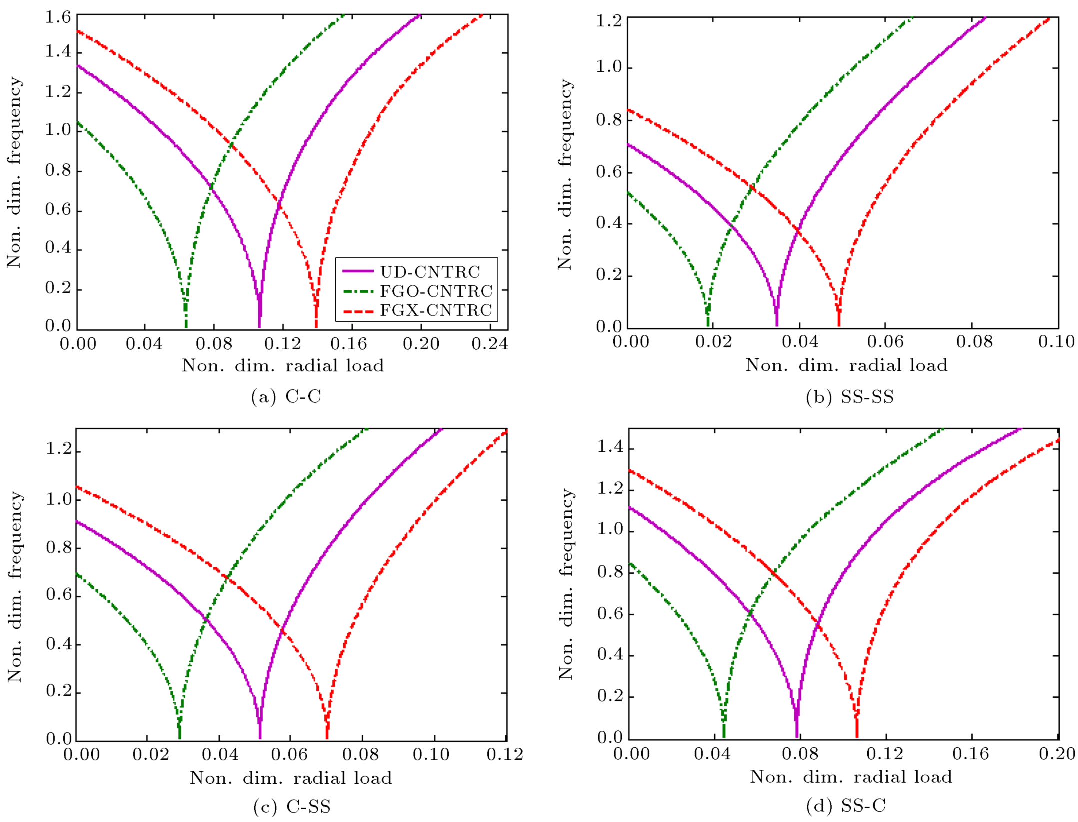

Figure 3. Vibration behavior of pre- and post-buckled FG-CNTRC annular plates for three different distributions of the CNTs ($b/h = 40, V_{cnt}^* = 0.17, a/b = 0.2$).

buckled state decrease with an increase in the radial load. This is because the stiffness of FG-CNTRC annular plates decreases by increasing the compressive radial loading. By increasing the compressive radial load to a new high, the stiffness matrix becomes a zero matrix at a certain point, called the buckling point. In this point, the FG-CNTRC annular plates do not experience any vibration and, consequently, the fundamental frequency is zero. It can be interpreted that the buckling point is a bifurcation point through which the FG-CNTRC annular plate meets its secondary equilibrium state known as the postbuckling region. Prior to the bifurcation point, the frequencies correspond to the pre-buckling configuration, and those after the critical buckling load are concerned with the vibration in the post-buckled state. For a buckled plate, it is seen that by increasing the compressive radial load, the fundamental frequencies increase. This implies that a buckled plate can withstand additional load without failure. In addition, it is deduced that the dimensionless frequency-load curves are continuous, yet not differentiable at the buckling point. According to this figure, it is observed that at a fixed value of radial load, the fundamental frequencies associated with the FGO-CNTRC plates have lower values than CNTRC annular plates with FGX and UD patterns in the pre-buckled region. While, in the postbuckled region, it is seen that the fundamental frequencies corresponding to FGO-CNTRC plates have larger values than the other two cases. It is due to this fact that the deflection in the postbuckled region intensifies the nonlinear stiffness matrices. In addition, it is implied that the effect of deflection is more significant than the CNT distribution pattern. Hence, at a certain point in the postbuckled region, since the deflection of FGO-CNTRC annular plate is more than two other distribution patterns, its frequency is greater than the annular plate with UD and FGX patterns.

Effects of V^*_{cnt} on the equilibrium postbuckling path and frequency-response curves are plotted in Figures 4 and 5 for the FGX-CNTRC annular plates. From these figures, it is seen that as V^*_{cnt} increases, the maximum dimensionless deflection decreases and critical buckling load increases. It means that by increasing V^*_{cnt}, the flexibility of the CNTRC annular plate increases, too. This is due to the considerable stiffness of CNTs. As it is expected, by increasing V^*_{cnt}, the frequencies of the CNTRC annular plates with FGX pattern increase in the pre-buckled region, whereas an opposite trend is observed for the postbuckling configuration.

Figures 6 and 7 show the effects of b/h on the maximum dimensionless deflection and frequency of the FGO-CNTRC plates with C-C, SS-SS, C-SS, and SS-C BCs, respectively. It is observed that an increase in b/h leads to increasing and decreasing the maximum

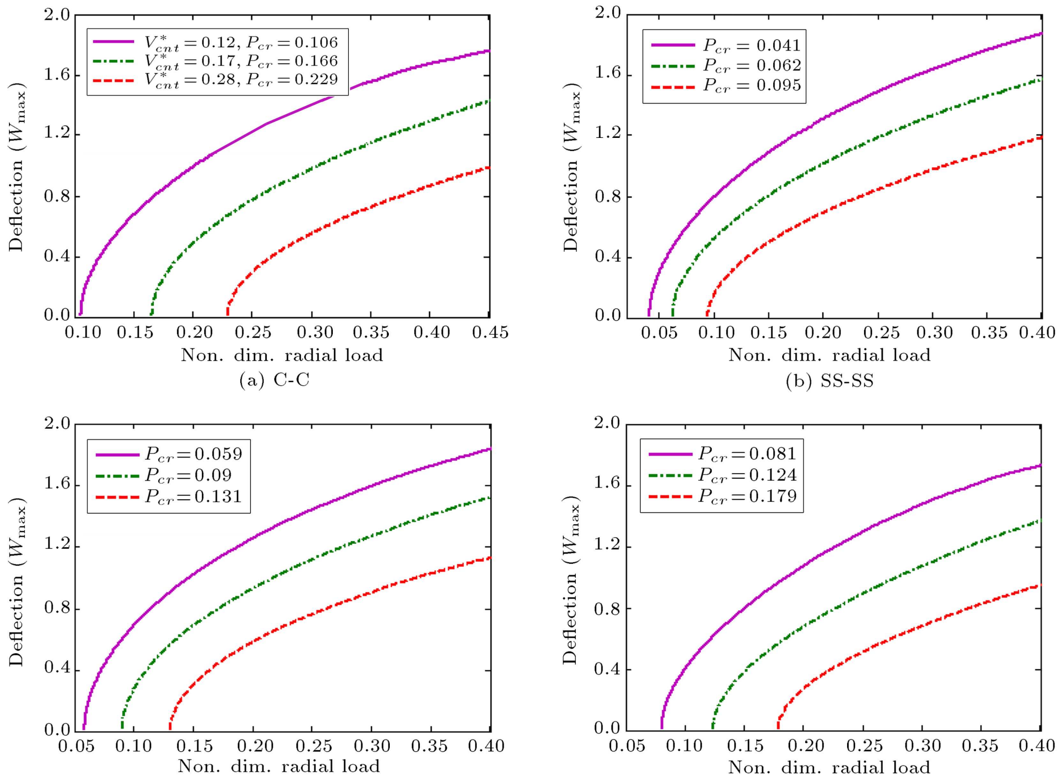

(a) C-C (b) SS-SS (c) C-SS (d) SS-C

Figure 4. Postbuckling path of FGX-CNTRC annular plates for different amounts of V^*_{cnt} $(b/h = 40, a/b = 0.3)$.

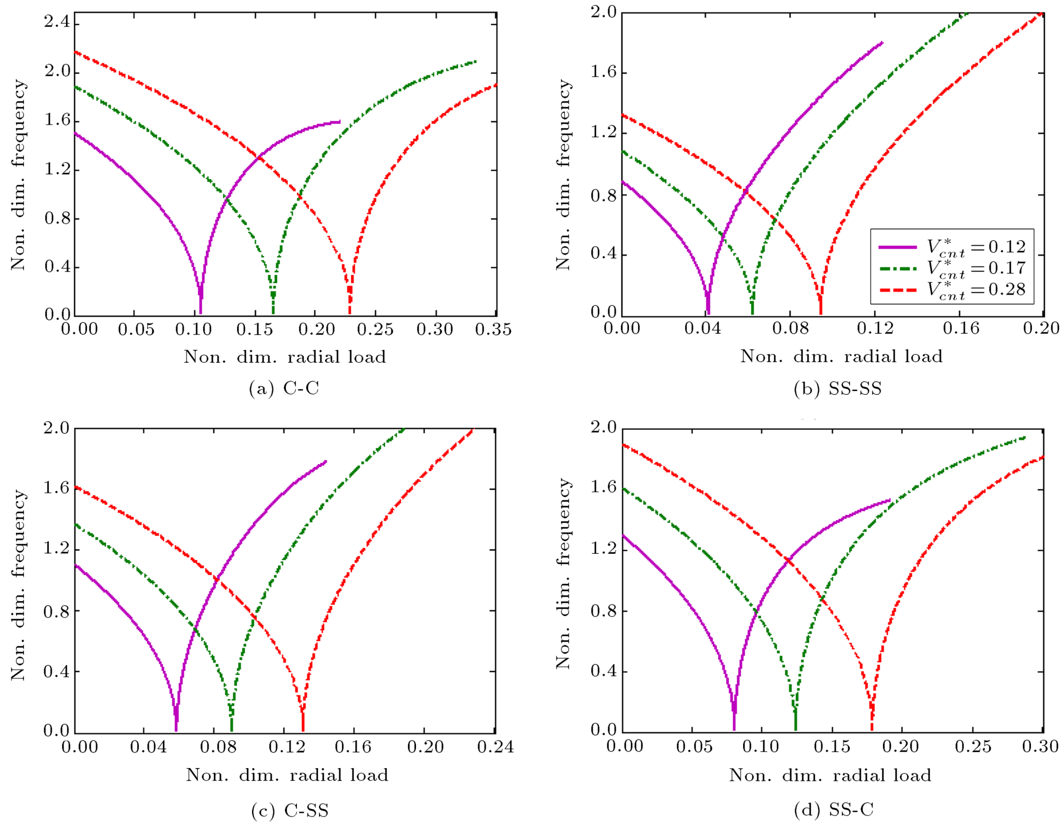

Figure 5. Free vibration of pre- and post-buckled FGX-CNTRC annular plates for various values of V^*_{cnt} $(b/h = 40, a/b = 0.3)$.

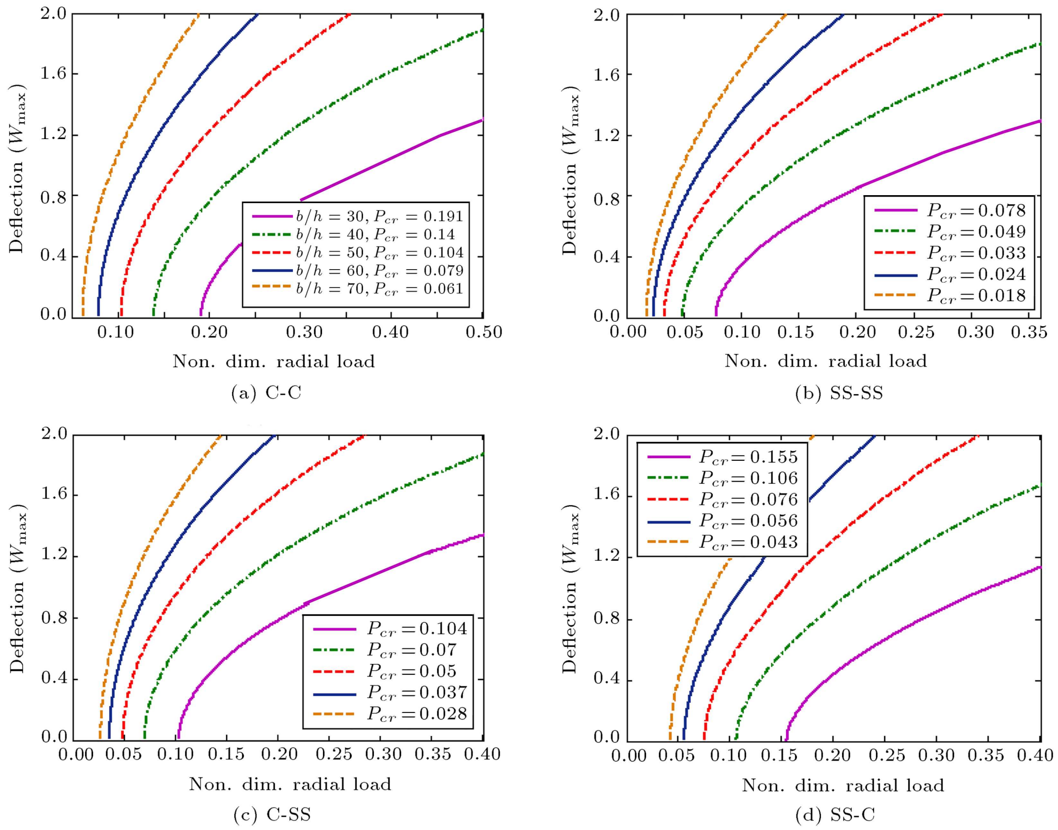

Figure 6. Postbuckling characteristics of FGX-CNTRC annular plates for various values of b/h $(V^*_{cnt} = 0.17, a/b = 0.2)$.

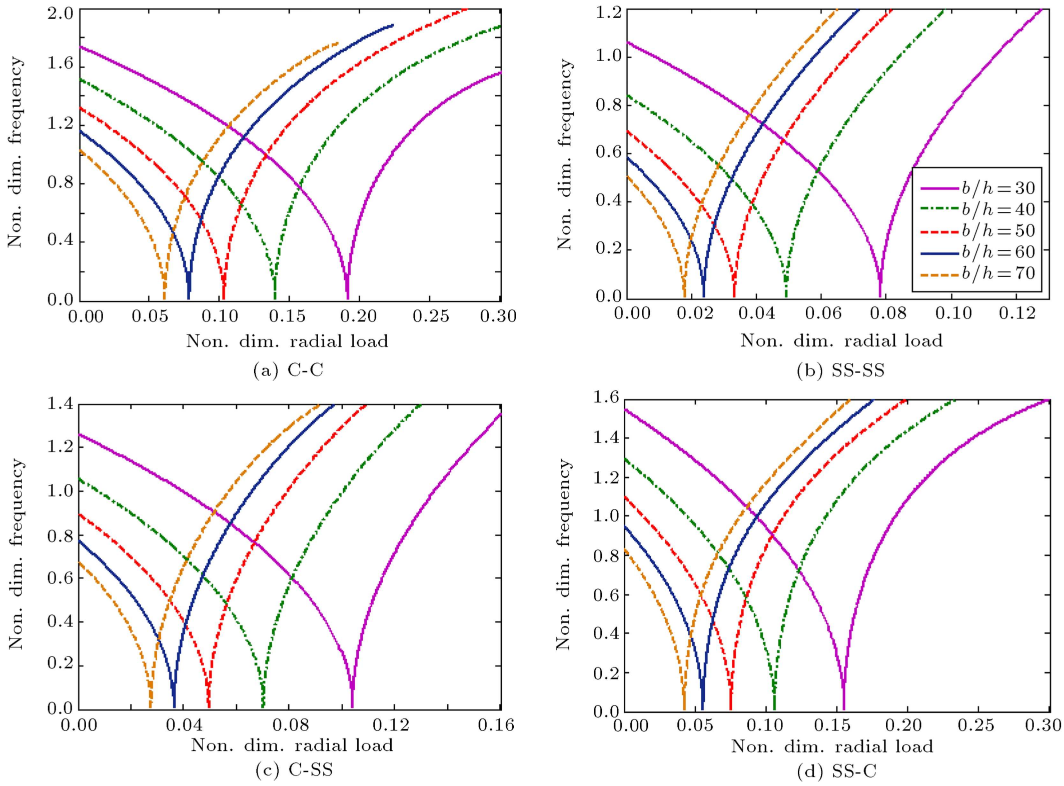

Figure 7. Free vibration response of pre- and post-buckled FGX-CNTRC annular plates for different values of b/h ($V^*_{cnt} = 0.17, a/b = 0.2$).

dimensionless deflection and the critical buckling load, respectively. In other words, an increase in b/h results in a decrease in the postbuckling load-carrying capacity of FGannular plates. According to the dimensionless frequency-radial load curves, it is seen that the frequency in the pre-buckled and post-buckled regions respectively decreases and increases as the plate aspect ratio rises.

Finally, the effects of a/b on the equilibrium postbuckling path and vibration characteristics of the FGX-CNTRC annular plates with C-C, SS-SS, C-SS, and SS-C BCs are shown in Figures 8 and 9, respectively. It is deduced that an increase in a/b decreases the maximum dimensionless deflection and increases the critical buckling load. In other words, the larger the difference between the outer and inner radii, the more stable the CNTRC plate. In addition, it is seen that increasing a/b causes the fundamental frequency to increase in the pre-buckled and deep post-buckled regions. In the post-buckled region, depending on the geometry and compressive radial loading (and, consequently, the deflection of plate), the fundamental frequency may decrease or increase.

5. Conclusion

In this study, a numerical methodology was adopted to investigate the postbuckling and free vibration of FG-CNTRC annular plates with different BCs. To this end, the FSDT along with the von Kármán geometric nonlinearity was utilized to formulate the underlying problem. The UD, FGO, and FGX distributions of SWCNTs in the composite plates were considered. Upon employing an equivalent continuum model, the material properties of FG-CNTRCs were estimated. Governing equations were attained by Hamilton's principle and, then, discretized by a GDQ-based method. Prior to examining the vibration behavior of post-buckled CNTRC plates, postbuckling analysis was performed to obtain the buckling load and equilibrium postbuckling path via the pseudo-arc length continuation scheme. Thereafter, the free vibration problem of the postbuckled CNTRC annular plates was solved as a standard linear eigenvalue equation. Effects of various parameters including types of BCs, CNT volume fraction, outer radius-to-thickness ratio, and inner-to-outer radius ratio on the postbuckling path and fundamental frequencies were investigated. Results showed that at a fixed value of the applied radial load, the fundamental frequencies of FGO-CNTRC plates are the smallest in the pre-buckling region and the largest in the post-buckling region among the given cases. In addition, it was observed that by increasing the outer radius-to-thickness aspect ratio, the fundamental frequencies increase in the prebuckling and deep postbuckling regions.

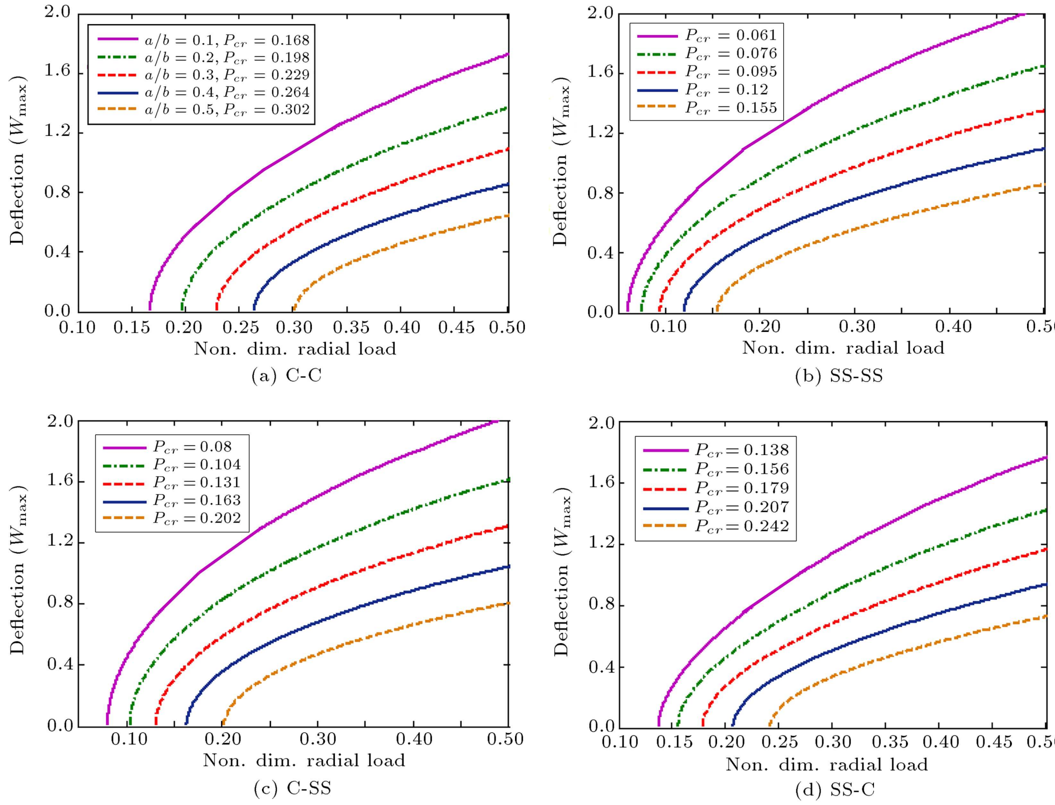

Figure 8. Postbuckling behavior of FGX-CNTRC annular plates for various values of a/b ($b/h = 40, V_{cnt}^* = 0.28$).

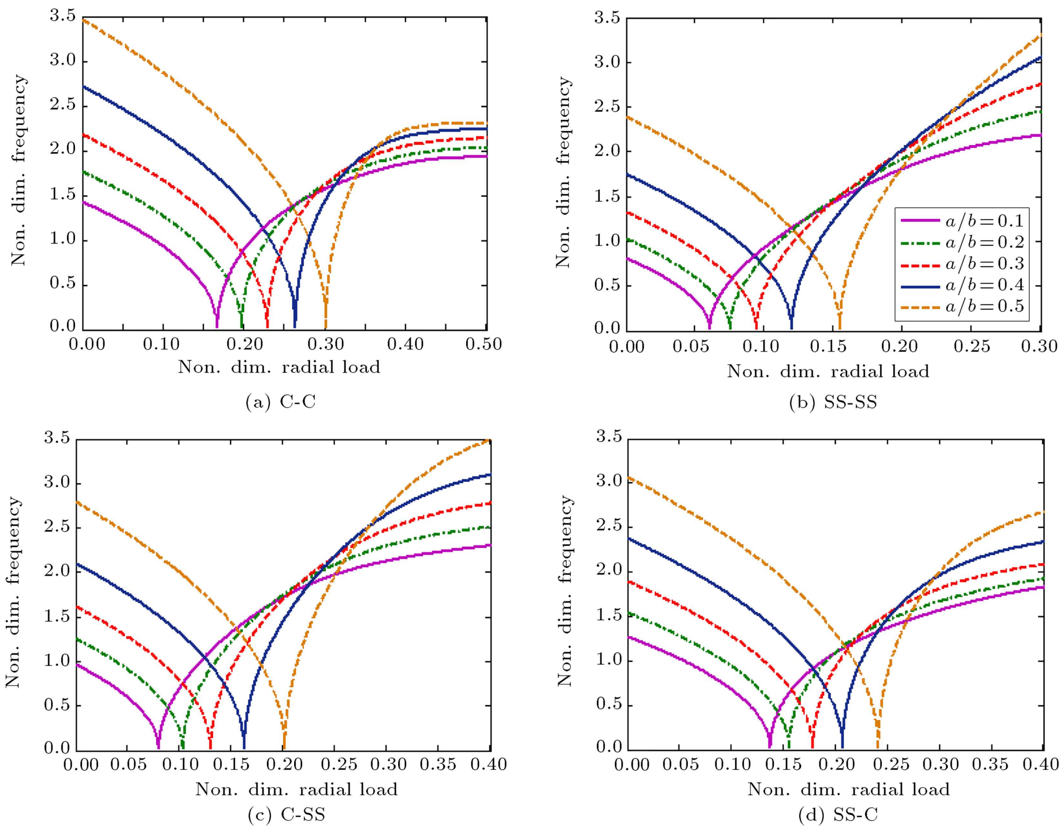

Figure 9. Vibration characteristics of pre- and post-buckled FGX-CNTRC annular plates for various values of a/b ($b/h = 40, V_{cnt}^* = 0.28$).

References

1. Iijima, S. "Helical microtubules of graphitic carbon", *Nature*, **354**, pp. 56-58 (1991).
2. Bianco, A., Kostarelos, K., and Prato, M. "Applications of carbon nanotubes in drug delivery", *Current Opinion in Chemical Biology*, **9**, pp. 674-679 (2005).
3. Treacy, M.J., Ebbesen, T., and Gibson, J. "Exceptionally high Young's modulus observed for individual carbon nanotubes", *Nature*, **381**, p. 678 (1996).
4. Baughman, R.H., Zakhidov, A.A., and De Heer, W.A. "Carbon nanotubes-the route toward applications", *Science*, **297**, pp. 787-792 (2002).
5. Salvetat, J.-P., Bonard, J.-M., Thomson, N., et al. "Mechanical properties of carbon nanotubes", *Applied Physics A,* **69**, pp. 255-260 (1999).
6. Li, Y., Wang, Q., and Wang, S. "A review on enhancement of mechanical and tribological properties of polymer composites reinforced by carbon nanotubes and graphene sheet: Molecular dynamics simulations", *Composites Part B: Engineering*, **160**, pp. 348-361 (2018).
7. Deep, N. and Mishra, P. "Evaluation of mechanical properties of functionalized carbon nanotube reinforced PMMA polymer nanocomposite", *Karbala International Journal of Modern Science*, **4**, pp. 207-215 (2018).
8. Hassanzadeh-Aghdam, M.K., Ansari, R., and Mahmoodi, M.J. "Thermo-mechanical properties of shape memory polymer nanocomposites reinforced by carbon nanotubes", *Mechanics of Materials*, **129**, pp. 80-98 (2019).
9. Ajayan, P., Stephan, O., Colliex, C., et al. "Aligned carbon nanotube arrays formed by cutting a polymer resin-nanotube composite", *Science*, **265**, pp. 1212-1214 (1994).
10. Hassanzadeh-Aghdam, M. and Mahmoodi, M. "A comprehensive analysis of mechanical characteristics of carbon nanotube-metal matrix nanocomposites", *Materials Science and Engineering: A*, **701**, pp. 34-44 (2017).
11. Hassanzadeh-Aghdam, M.K., Ansari, R., and Mahmoodi, M.J. "Thermal expanding behavior of carbon nanotube-reinforced metal matrix nanocomposites-A micromechanical modeling", *Journal of Alloys and Compounds*, **744**, pp. 637-650 (2018).
12. Hassanzadeh-Aghdam, M., Ansari, R., and Mahmoodi, M. "Micromechanical estimation of biaxial thermo-mechanical responses of hybrid fiber-reinforced metal matrix nanocomposites containing carbon nanotubes", *Mechanics of Materials*, **119**, pp. 1-15 (2018).
13. Foroughi, M.R., Khoroushi, M., Nazem, R., et al. "The effect of carbon nanotubes/bioglass nanocomposite on mechanical and bioactivity properties of glass ionomer cement", *Scientia Iranica*, **23**, pp. 3123-3134 (2016).
14. AfzaliTabara, M., Alaeib, M., Khojasteha, R.R., et al. "Preference of nanoporous graphene to Single-Walled Carbon Nanotube (SWCNT) for preparing silica nanohybrid Pickering emulsion for potential Chemical Enhanced Oil Recovery (C-EOR)", *Scientia Iranica*, **24**, pp. 3491-3499 (2017).
15. Rafiee, M., Nitzsche, F., and Labrosse, M. "Effect of functionalization of carbon nanotubes on vibration and damping characteristics of epoxy nanocomposites", *Polymer Testing*, **69**, pp. 385-395 (2018).
16. Nasihatgozar, M., Daghigh, V., Eskandari, M., et al. "Buckling analysis of piezoelectric cylindrical composite panels reinforced with carbon nanotubes", *International Journal of Mechanical Sciences*, **107**, pp. 69-79 (2016).
17. Wu, H., Kitipornchai, S., and Yang, J. "Imperfection sensitivity of thermal post-buckling behaviour of functionally graded carbon nanotube-reinforced composite beams", *Applied Mathematical Modelling*, **42**, pp. 735-752 (2017).
18. Wu, H.L., Kitipornchai, S., and Yang, J. "Thermal buckling and postbuckling analysis of functionally graded carbon nanotube-reinforced composite beams", *Applied Mechanics and Materials*, **846**, p. 182 (2016).
19. Wang, M., Li, Z.-M., and Qiao, P. "Semi-analytical solutions to buckling and free vibration analysis of carbon nanotube-reinforced composite thin plates", *Composite Structures*, **144**, pp. 33-43 (2016).
20. Alibeigloo, A. and Liew, K. "Elasticity solution of free vibration and bending behavior of functionally graded carbon nanotube-reinforced composite beam with thin piezoelectric layers using differential quadrature method", *International Journal of Applied Mechanics*, **7**, pp. 1550002 (2015).
21. Jalali, S. and Heshmati, M. "Buckling analysis of circular sandwich plates with tapered cores and functionally graded carbon nanotubes-reinforced composite face sheets", *Thin-Walled Structures*, **100**, pp. 14-24 (2016).
22. Mehar, K., Panda, S.K., and Mahapatra, T.R. "Thermoelastic deflection responses of CNT reinforced sandwich shell structure using finite element method", *Scientia Iranica*, **25**, pp. 2722-2737 (2018).
23. Hassanzadeh-Aghdam, M., Mahmoodi, M., and Ansari, R. "Micromechanical characterizing the effective elastic properties of general randomly distributed CNT-reinforced polymer nanocomposites", *Probabilistic Engineering Mechanics*, **53**, pp. 39-51 (2018).
24. Hassanzadeh-Aghdam, M., Mahmoodi, M., and Ansari, R. "Micromechanics-based characterization of mechanical properties of fuzzy fiber-reinforced composites containing carbon nanotubes", *Mechanics of Materials*, **118**, pp. 31-43 (2018).
25. Griebel, M. and Hamaekers, J. "Molecular dynamics simulations of the elastic moduli of polymer-carbon nanotube composites", *Computer Methods in Applied Mechanics and Engineering*, **193**, pp. 1773-1788 (2004).

26. Han, Y. and Elliott, J. "Molecular dynamics simulations of the elastic properties of polymer/carbon nanotube composites", *Computational Materials Science*, **39**, pp. 315-323 (2007).

27. Bonnet, P., Sireude, D., Garnier, B., et al. "Thermal properties and percolation in carbon nanotube-polymer composites", *Applied Physics Letters*, **91**, p. 201910 (2007).

28. Meguid, S. and Sun, Y. "On the tensile and shear strength of nano-reinforced composite interfaces", *Mater. Design.*, **25**, pp. 289-296 (2004).

29. Vodenitcharova, T. and Zhang, L. "Bending and local buckling of a nanocomposite beam reinforced by a single-walled carbon nanotube", *International Journal of Solids and Structures*, **43**, pp. 3006-3024 (2006).

30. Gholami, R., Ansari, R., and Gholami, Y. "Nonlinear resonant dynamics of geometrically imperfect higher-order shear deformable functionally graded carbon-nanotube reinforced composite beams", *Composite Structures*, **174**, pp. 45-58 (2017).

31. Formica, G., Lacarbonara, W., and Alessi, R. "Vibrations of carbon nanotube-reinforced composites", *Journal of Sound and Vibration*, **329**, pp. 1875-1889 (2010).

32. Ansari, R., Shojaei, M.F., Mohammadi, V., et al. "Nonlinear forced vibration analysis of functionally graded carbon nanotube-reinforced composite Timoshenko beams", *Composite Structures*, **113**, pp. 316-327 (2014).

33. Shen, H.-S. and He, X. "Large amplitude free vibration of nanotube-reinforced composite doubly curved panels resting on elastic foundations in thermal environments", *Journal of Vibration and Control*, **23**, pp. 2672-2689 (2017).

34. Ansari, R., Hasrati, E., Shojaei, M.F., et al. "Forced vibration analysis of functionally graded carbon nanotube-reinforced composite plates using a numerical strategy", *Physica E: Low-dimensional Systems and Nanostructures*, **69**, pp. 294-305 (2015).

35. Ansari, R. and Gholami, R. "Nonlinear primary resonance of third-order shear deformable functionally graded nanocomposite rectangular plates reinforced by carbon nanotubes", *Composite Structures*, **154**, pp. 707-723 (2016).

36. Ansari, R., Pourashraf, T., Gholami, R., and Shahabodini, A. "Analytical solution for nonlinear postbuckling of functionally graded carbon nanotube-reinforced composite shells with piezoelectric layers", *Composites Part B: Engineering*, **90**, pp. 267-277 (2016).

37. Lin, F. and Xiang, Y. "Numerical analysis on nonlinear free vibration of carbon nanotube reinforced composite beams", *International Journal of Structural Stability and Dynamics*, **14**, p. 1350056 (2014).

38. Song, Z., Zhang, L., and Liew, K. "Vibration analysis of CNT-reinforced functionally graded composite cylindrical shells in thermal environments", *International Journal of Mechanical Sciences*, **115**, pp. 339-347 (2016).

39. Mehrabadi, S.J., Aragh, B.S., Khoshkhahesh, V., et al. "Mechanical buckling of nanocomposite rectangular plate reinforced by aligned and straight single-walled carbon nanotubes", *Composites Part B: Engineering*, **43**, pp. 2031-2040 (2012).

40. Lei, Z., Liew, K., and Yu, J. "Free vibration analysis of functionally graded carbon nanotube-reinforced composite plates using the element-free kp-Ritz method in thermal environment", *Composite Structures*, **106**, pp. 128-138 (2013).

41. Shen, H.-S., Wang, H., and Yang, D.-Q. "Vibration of thermally postbuckled sandwich plates with nanotube-reinforced composite face sheets resting on elastic foundations", *International Journal of Mechanical Sciences*, **124**, pp. 253-262 (2017).

42. Ahmadi, M., Ansari, R., and Rouhi, H. "Studying buckling of composite rods made of hybrid carbon fiber/carbon nanotube reinforced polyimide using multiscale FEM", *Scientia Iranica, Transactions B* (In Press). DOI:10.24200/sci.2018.5722.1444

43. Gholami, R. and Ansari, R. "Geometrically nonlinear resonance of higher-order shear deformable functionally graded carbon-nanotube-reinforced composite annular sector plates excited by harmonic transverse loading", *The European Physical Journal Plus*, **133**, p. 56 (2018).

44. Gholami, R., Ansari, R., and Gholami, Y. "Numerical study on the nonlinear resonant dynamics of carbon nanotube/fiber/polymer multiscale laminated composite rectangular plates with various boundary conditions", *Aerospace Science and Technology*, **78**, pp. 118-129 (2018).

45. Wang, Q., Pang, F., Qin, B., et al. "A unified formulation for free vibration of functionally graded carbon nanotube reinforced composite spherical panels and shells of revolution with general elastic restraints by means of the Rayleigh-Ritz method", *Polymer Composites*, **39**, pp. E924-E944 (2018).

46. Esawi, A.M. and Farag, M.M. "Carbon nanotube reinforced composites: potential and current challenges", *Mater. Design.*, **28**, pp. 2394-2401 (2007).

47. Fidelus, J., Wiesel, E., Gojny, F., et al. "Thermo-mechanical properties of randomly oriented carbon/epoxy nanocomposites", *Composites Part A: Applied Science and Manufacturing*, **36**, pp. 1555-1561 (2005).

48. Shen, H.-S. "Nonlinear bending of functionally graded carbon nanotube-reinforced composite plates in thermal environments", *Composite Structures*, **91**, pp. 9-19 (2009).

49. Librescu, L., Oh, S.-Y., and Song, O. "Thin-walled beams made of functionally graded materials and operating in a high temperature environment: vibration and stability", *Journal of Thermal Stresses*, **28**, pp. 649-712 (2005).

50. Shen, H.-S. and Wang, Z.-X. "Assessment of Voigt and Mori-Tanaka models for vibration analysis of

functionally graded plates", *Composite Structures*, **94**, pp. 2197-2208 (2012).

51. Shen, H.-S. "Nonlinear vibration of shear deformable FGM cylindrical shells surrounded by an elastic medium", *Composite Structures*, **94**, pp. 1144-1154 (2012).
52. Wang, Z.-X. and Shen, H.-S. "Nonlinear vibration of nanotube-reinforced composite plates in thermal environments", *Computational Materials Science*, **50**, pp. 2319-2330 (2011).
53. Liew, K.-M., Xiang, Y., Kitipornchai, S., et al., *Vibration of Mindlin Plates: Programming the p-Version Ritz Method*, Elsevier (1998).
54. Reddy, J.N., *Mechanics of Laminated Composite Plates and Shells: Theory and Analysis*, CRC press (2004).
55. Gürarslan, G. and Sari, M. "Numerical solutions of linear and nonlinear diffusion equations by a differential quadrature method (DQM)", *International Journal for Numerical Methods in Biomedical Engineering*, **27**, pp. 69-77 (2011).
56. Bellman, R. and Casti, J. "Differential quadrature and long-term integration", *Journal of Mathematical Analysis and Applications*, **34**, pp. 235-238 (1971).
57. Shu, C., *Generalized Differential-Integral Quadrature and Application to the Simulation of Incompressible Viscous Flows Including Parallel Computation*, University of Glasgow (1991).
58. Shu, C. and Richards, B.E. "Application of generalized differential quadrature to solve two-dimensional incompressible Navier-Stokes equations", *International Journal for Numerical Methods in Fluids*, **15**, pp. 791-798 (1992).
59. Ansari, R., Gholami, R., Shojaei, M.F., et al. "Coupled longitudinal-transverse-rotational free vibration of post-buckled functionally graded first-order shear deformable micro-and nano-beams based on the Mindlin's strain gradient theory", *Applied Mathematical Modelling*, **40**, pp. 9872-9891 (2016).
60. Chen, W. and Zhong, T. "The study on the nonlinear computations of the DQ and DC methods", *Numerical Methods for Partial Differential Equations: An International Journal*, **13**, pp. 57-75 (1997).
61. Shen, H.-S. and Zhang, C.-L. "Thermal buckling and postbuckling behavior of functionally graded carbon nanotube-reinforced composite plates", *Mater. Design.*, **31**, pp. 3403-3411 (2010).
62. Ke, L.-L., Yang, J., Kitipornchai, S., et al. "Axisymmetric postbuckling analysis of size-dependent functionally graded annular microplates using the physical neutral plane", *International Journal of Engineering Science*, **81**, pp. 66-81 (2014).

Biographies

Raheb Gholami received his BS, MS, and PhD degrees in Mechanical Engineering from University of Guilan, Rasht, Iran in 2008, 2010, and 2015, respectively. He is currently a faculty member at the Department of Mechanical Engineering, Lahijan Branch, Islamic Azad University. His research background and interests include computational micro- and nanomechanics, numerical techniques, nonlinear analyses, and prediction of mechanical behavior of beam, plate and shell-type structures.

Reza Ansari received his PhD degree from University of Guilan, Rasht, Iran in 2008, where he is currently a faculty member at the Faculty of Mechanical Engineering. During his PhD program, he was also a visiting fellow at Wollongong University, Australia from 2006 to 2007. He has authored more than 400 refereed journal papers and 12 book chapters. His research background and interests include computational mechanics, numerical analysis, continuum mechanics, nano-, micro-, and macro-mechanics.